578642

Sandia National Laboratories

Operated for the United States Department of Energy
by National Technology and Engineering Solutions
of Sandia, LLC.

Albuquerque, New Mexico 87185-0101
Livermore, California 94551-0969

date: December 2, 2022

to: SNL WIPP[1] Records Center, SNL WIPP Geochemistry
Sandia National Laboratories
4100 National Parks Highway, Building A, Carlsbad, New Mexico 88220, U.S.A.

from: Jay Jang (jjang@sandia.gov)
Sandia National Laboratories
4100 National Parks Highway, Building A, Carlsbad, New Mexico 88220, U.S.A.

subject: The $PbCO_3(s)$ - $NaHCO_3$ - Na_2CO_3 - H_2O Experiment (Revision 0): Addendum to Xiong (2015a,b)

I. DRIVERS

This memo re-evaluates the measurements and model parameterization of Xiong (2015a,b). The measurements of solution chemistry obtained from the $PbCO_3(s)$ - $NaHCO_3$ - Na_2CO_3 - H_2O experiment were reported in Kirkes et al. (2014a,b,c). Kirkes et al. (2014c) is the updated version of Kirkes et al. (2014a,b). The goal of the experiment was to measure the solubility of $PbCO_3(s)$ (cerussite) in aqueous solutions containing mixture of two salts, $NaHCO_3$ and Na_2CO_3. The measurements and model parameterization of the solution chemistry were presented in Xiong (2015a,b). Xiong (2015a) and Xiong (2015b) parameterized the same set of measurements, and the set of log Ks and PIPs in Xiong (2015b) is different from Xiong (2015a).

Xiong (2015a,b) were completed prior to the characterization of the final solid product(s) in 2019 (Kirkes and Xiong, 2019). The XRD scans reported in Kirkes and Xiong (2019) for the experiments in Xiong (2015a,b) are dated to 2018. In Xiong (2015b), there exists a statement claiming no solid phase change identified by XRD, but the corresponding XRD scans were not presented therein and cannot be tracked. It is unclear whether the XRD scans in Kirkes and Xiong (2019) are the first ones or repeated ones of the XRDs mentioned in Xiong (2015b).

[1] SNL WIPP: Sandia National Laboratories at the Waste Isolation Pilot Plant (WIPP). WIPP is located ~26 miles southeast of Carlsbad, New Mexico, U.S.A., built 2,150 feet underground in the Salado Formation, a thick Permian evaporite deposit in the northern Delaware Basin.

Exceptional Service in the National Interest

Information Only

Na^+ was considered as a non-reactive/conservative species in Xiong (2015a,b), while the ΣNa measurements reported in Kirkes et al. (2014a,b,c) indicated the removal of Na^+ from solutions,[2] suggesting the occurrence of parallel precipitation reaction(s) involving Na^+, which include the formation of $NaPb_2(CO_3)_2(OH)$(s) (abellaite) at the expense of the added $PbCO_3$(s) (cerussite). The ΣNa and ΣCO3 values reported in Xiong (2015a,b) were not traceable to Scientific Notebooks, and the ΣPb measurements were reported in incorrect units in Xiong (2015a,b) as imported from Kirkes et al. (2014a,b,c).

The model parameterization of Xiong (2015a,b) seems to have been performed under an assumption that the initially added $PbCO_3$(s) (cerussite) did not change throughout the aging time. In other words, the solubility constant of cerussite was fitted to the solution chemistry measurements without identifying the solid at the end of experiments.

The $PbCO_3$(s) (cerussite) has transformed to $NaPb_2(CO_3)_2(OH)$(s) (abellaite) as reported in Kirkes and Xiong (2019). Thus, the author of Xiong (2015a,b) would have known what to do based on the finding of Kirkes and Xiong (2019). For example, corrections or addenda should have been issued for Xiong (2015a,b) after the findings in Kirkes and Xiong (2019) were reported. It is unclear if any follow up actions were initiated since 2019.

The set of experiments analyzed in this memo was installed on 7/27/2010 (date of entries in WIPP-Solubility-12, page 30; Excerpt IV-1 on page 7). The last measurements documented in Kirkes et al. (2014c) are dated on July of 2012 with the aging time of 720 days since the initiation of the experiments on 7/27/2010 (Table V-1, Table V-3, Table V-5, Table V-7). The solid characterization was conducted in August of 2018.

There exists an extra set of measurements documented in Scientific Notebooks (Table I-1). They are valid measurements under SNL WIPP QA, and were found after the completion of the model parameterization in Section VIII. When they are compared with the statistics in Table V-2, Table V-4, Table V-6, and Table V-8, no significant differences were observed. So, the statistics in Table V-2, Table V-4, Table V-6, and Table V-8 were not modified.

They were produced in 7/30/2014 - 4/21/2016 after the aging time exceeding 1460 days by 7/30/2014 (up to 2090 days by 4/21/2016) counted from the installation date (7/27/2010; WIPP-Solubility-12, page 30; Excerpt IV-1). Therefore, the time elapse between the last set of measurements documented in

[2] Refer to Section V.4 starting in page 16 and Section VII starting in page 21 to find out how the ΣNa measurements known in Kirkes et al. (2014a,b,c) could have been used in Xiong (2015a,b) if the ΣNa values published in Xiong (2015a,b) had been verified with respect to the measurements and loadings.

Information Only

Kirkes et al. (2014c) (up to 720 days) and the measurements in Table I-1 (1460 days) is 740 days, which is as long as the aging time documented in Kirkes et al. (2014c) (720 days). In other word, the set of experiments of concern of this memo was aged for 1460 days (for 2090 days for carbonate measurement) in total.

Table I-1. Extra measurements produced between Xiong (2015a,b) and Kirkes and Xiong (2019). The values in italic font are outside the ranges defined in the Tables identified at the bottom row.

Reactor ID	pHr	ΣPb, M	ΣCO3, M	ΣNa, M
PbCO3-Buffer A-1	*9.81*	1.98E-05	8.36E-02	1.25E-01
PbCO3-Buffer A-2	*9.81*	*1.91E-05*	8.43E-02	1.27E-01
PbCO3-Buffer B-1	*9.74*	5.18E-05	*2.74E-01*	*3.46E-01*
PbCO3-Buffer B-2	*9.72*	5.01E-05	2.53E-01	3.68E-01
PbCO3-Buffer C-1	*9.71*	1.79E-04	*3.25E-01*	1.10E+00
PbCO3-Buffer C-2	*9.76*	1.91E-04	6.67E-01	1.09E+00
PbCO3-Buffer D-1	*9.79*	3.58E-04	9.45E-01	1.68E+00
PbCO3-Buffer D-2	*9.81*	3.90E-04	1.00E+00	1.76E+00
PbCO3-Buffer E-1	*9.85*	8.42E-04	1.48E+00	2.79E+00
PbCO3-Buffer E-2	*9.84*	7.47E-04	*1.51E+00*	2.60E+00
PbCO3-Buffer F-1	*9.85*	6.40E-04	1.62E+00	2.80E+00
PbCO3-Buffer F-2	*9.85*	8.35E-04	1.55E+00	2.91E+00
Source	WIPP-Solubility-27, p.79	WIPP-Solubility-37, p.83	WIPP-Solubility-46, p.67, 68	WIPP-Solubility-37, p.80
Date of measurements	7/30/2014	8/20/2014	4/21/2016	8/14/2014
Number of exceptions from the ranges defined in Table N-n (page x)	12	1	2	0
	Table V-2 (12)	Table V-4 (14)	Table V-6 (16)	Table V-8 (18)

The ΣCO3 measured after more than 2090 days of aging exhibit two exceptions out of 12 measurements (see column of ΣCO3 in Table I-1) from the 95% confidence interval defined in Table V-6 on page 16. Note that the date of measurements for ΣCO3 is 4/21/2016, even later than the dates of measurements for ΣPb and ΣNa. The ΣPb and ΣNa exhibit less number of exceptions (one and zero; Table I-1). See Figure V-6 for the accuracy and precision of the ΣCO3 measurements, and also see discussion in Section VII on the rationales for the minimized loss of ΣCO3 via the escape of CO_2(g). The change of carbonate concentrations was insignificant and the concentrations were stable for up to 2090 days of aging.

The mineralogical transformation of $PbCO_3$(s) (cerussite) to $NaPb_2(CO_3)_2(OH)$(s) (abellaite) consumes Na^+ from the solution. Refer to Reaction (1) on page 22. Therefore, the consistent ΣNa throughout 1460 days of aging indicate that the further formation of abellaite at the expense of the added cerussite has effectively stopped over the initial 720 days of aging (probably much earlier than 720 days; see the

Information Only

plateaus of ΣNa in Figure V-7 on page 17), which is the total aging time up to the last measurements documented in Kirkes et al. (2014c). The minimized transformation over 720 - 1460 days of aging might be registered in the consistent negative shift of pH measured at 1460 days of aging via Reaction (1), i.e., 12 out of 12 measurements of pHr in Table I-1 negatively deviated from the range defined in Table V-2 by less than 0.1 pH unit. However, the less than 0.1 pH unit difference in pHr is small enough to be considered the shift of the measurement.

Therefore, during the aging time inclusive of the extra measurements (Table I-1; up to 1460 days, i.e., from 7/27/2010 to 7/30/2014; up to 2090 days for carbonate measurement), it can be stated that the set of reactors has been in the solubility equilibrium of abellaite. During the days from 7/30/2014 to August 2018 of the XRD scans (another ~1450 days), the expected event in the reactors would be the evaporation of water due to diffusion of water vapor through the plastic or the thread of the bottle between cap.

The evaporation of water could have resulted in the increase of the dissolved concentrations of $NaHCO_3$ and Na_2CO_3, however, since they consist of the pH buffer, the shift of pH is not expected without orders of magnitude increase of the salts or selective/non-stoichiometric precipitation of either $NaHCO_3$ or Na_2CO_3.

As governed by Reaction (1) in page 22, the mineral paragenesis of $PbCO_3$(s) (cerussite) and $NaPb_2(CO_3)_2(OH)$(s) (abellaite) is not a function of dissolved carbonate concentration. From the XRD scans (Figure VI-1 on page 21), no peaks of $NaHCO_3$ or Na_2CO_3 are observed, indicating that the increase of the dissolved concentrations of $NaHCO_3$ and Na_2CO_3 due to water evaporation was not enough to condensate and precipitate out the salts, proving that the salts stayed in aqueous phase without precipitation until the date of solid characterization in August of 2018.

Therefore, the stable pHr, ΣPb, ΣNa, and ΣCO3 for 1460 days indicate that the formation of $NaPb_2(CO_3)_2(OH)$(s) (abellaite) has been complete and in equilibrium, and the potential water evaporation during the storage could not affect the solid-solution equilibrium due to the tight pH buffering of the salts for 2927 days (from installation on 7/27/2010 to XRDs in August 2018). Thus, the XRDs in Kirkes and Xiong (2019) that identify the formation of $NaPb_2(CO_3)_2(OH)$(s) (abellaite) are valid observation representing the solid phase in equilibrim with the aqueous phase throughout the entire aging time (c.f., Kirkes and Xiong, 2019, pages 16 and 17).

The incomplete data interpretation and model parameterization in Xiong (2015a,b) resulted in the creation of a unique log K of $PbCO_3$(s) (cerussite) that makes cerussite less soluble than reported in the

Information Only

literature. The less soluble cerussite is designated as a possible constituent for the passivation layer for lead corrosion in Xiong et al. (2021a). Xiong et al. (2021a) is cited in Xiong (2022, Chapter 3 ...) to evaluate the corrosion mechanism of lead in carbonate- and sulfide-bearing solutions. Making cerussite less soluble means a wider stability field of cerussite when cerussite competes with other lead-containing minerals, e.g., galena (Xiong, 2022, Chapter 3 ..). The unique log K of cerussite in Xiong (2015a,b) would widen the stability field of cerussite over galena, making cerussite look like an apparently plausible candidate for a passivation layer phase in lead corrosion.

Mechanism and products of lead and iron corrosion is an on-going research topic of SNL WIPP Geochemistry. After a courtesy review of Xiong (2022, Chapter 3 ..) in February 2022 (Miller, 2022), SNL WIPP Geochemistry requested to untie Xiong (2022, Chapter 3 ..) from the on-going efforts of SNL WIPP Geochemistry (Jang, 2022). However, the author of Xiong (2022, Chapter 3 ..) claimed that the book chapter contains no ties to SNL WIPP Geochemistry (Shoemaker, 2022). The book chapter is now a Sandia Report (SAND2022-2827B) available outside SNL WIPP Geochemistry.

The book chapter (Xiong, 2022, Chapter 3 ..) is back referenced to CRA-2019 through "Xiong (2015a,b)", and tied to SNL WIPP Geochemistry by the following chain of references:

Kirkes et al. (2014a,b,c) → "Xiong (2015a,b)" → Xiong et al. (2021a) → Xiong (2022, Chapter 3 ..)

As of 4/18/2022, Xiong (2015a,b) are listed as references for CRA-2019 at "https://wipp.energy.gov/library/CRA/CRA%202019/referencesList.html#X". However, SNL WIPP Geochemistry will throughly evaluate the technical accuracy of lead-carbonate system for future CRA, and this memo is one of the evaluation efforts.

This memo presents comprehensive data processing/interpretation and model parameterization, so that SNL WIPP Geochemistry can untie the references below in gray font:

Kirkes et al. (2014a,b,c) → "This memo" // Xiong (2015a,b) → Xiong et al. (2021a) → Xiong (2022, Chapter 3 ..)

This way, SNL WIPP Geochemistry unties Xiong (2015a,b), Xiong et al. (2021a), and Xiong (2022, Chapter 3 ..) from its on-going research, and makes Xiong (2015a,b), Xiong et al. (2021a), and Xiong (2022, Chapter 3 ..) standing-alone documents. Xiong (2015a,b) are just two of numerous instances

Information Only

where (i) the data processing/interpretation were performed in unique ways, and (ii) the data were not reproduced with improved experimental protocols.[3]

Through this memo, SNL WIPP Geochemistry presents a comprehensive data processing/interpretation and model parameterization of the same solution chemistry measurements in Kirkes et al. (2014a,b,c) and solid identification results in Kirkes and Xiong (2019) for the $PbCO_3$(s) - $NaHCO_3$ - Na_2CO_3 - H_2O experiment. Incorrect concentration unit used for the experiments in Xiong (2015a,b) and Kirkes et al. (2014a,b,c) was corrected. This is a part of SNL WIPP Geochemistry's on-going efforts for (i) accurate, traceable, and transparent data processing/interpretation and model parameterization, and (ii) establishing accuracy and precision of instrumental measurements.

The difference between this memo and Xiong (2015a,b) are explained in detail in Section IX.2 that was once placed right before Section X. REFERENCES. Interested readers may skip the following sections and directly visit the Section IX.2.

The data processing/interpretation of this memo replaces Table 3 of Xiong (2015a) and Table 2 of Xiong (2015b), where not-so-good-looking data are arbitrarily omitted without justifications (Excerpt IX-4 and Excerpt IX-5 in Section IX.2). The model parameterization of this memo invalidates the log K for cerussite of -13.65 in Xiong (2015a) and -13.76 in Xiong (2015b). Consequently, the PIPs[4] derived in Xiong (2015a,b) in relation to the aforementioned unique log Ks are not valid.

Based on this memo, Xiong (2015a,b) won't be considered for the calculations related to the compliance decision making processes. As of 4/18/2022, Xiong (2015a,b) are listed as references for CRA-2019 at "https://wipp.energy.gov/library/CRA/CRA%202019/referencesList.html#X".

II. Chemical System

A lead carbonate solid, $PbCO_3$(s) (cerussite), was added to solutions containing both $NaHCO_3$ and Na_2CO_3. The five system components are Pb^{+2}, HCO_3^-, Na^+, H^+, and H_2O.

III. Goals and Hypotheses

The goals of these chloride-free solubility experiments were the following: (i) to measure solubility of $PbCO_3$(s) (cerussite) in carbonate solutions, and (ii) to see how the common ion effect influences the

[3] Pb-EDTA work in Xiong (2014); Fe-B in Xiong et al., (2018a); Nd(OH)3(s) work in Xiong et al. (2016, 2017a); Pb-Oxalate, Ca-EDTA, Ca-Citrate works in Xiong (2015c, 2017b, 2018b) and Xiong (2021b); Nd-B work in Kirkes and Hora (2020).
[4] PIPs: Pitzer Interaction Parameters.

Information Only

dissolution of $PbCO_3$(s) (cerussite) within a narrow pHr range of bicarbonate/carbonate buffer solutions, the common-ion being CO_3^{-2}.

IV. Reactor Preparation

Experiments and measurements were performed at ambient temperature under the building temperature control (24.5 ± 4.3 °C) (Arnold and Jang, 2022). The experiments were prepared under six different conditions in duplicate, i.e., six different loadings of mixture of two salts, $NaHCO_3$ and Na_2CO_3. Thus, 12 reactors were prepared in total. The preparation in Excerpt IV-1 was verified by tracing back to the Scientific Notebooks maintained under SNL WIPP QA. The differences noticed from the loaded concentrations of $NaHCO_3$ and Na_2CO_3 in Excerpt IV-1 and Excerpt IV-2 were the motivation of this re-verification effort. Solution preparation described in Excerpt IV-3 indicated that the 1000-mL volumetric flask was used to determine the mass of the DI water by volume, not to determine the final volume of the solutions. Therefore, 1000 mL DI ≡ 0.997 kg of water was mixed with the prescribed mass of the two salts at 25 °C, assuring that the unit of loaded concentrations of the two salts are molality, not Molarity.

The verified concentrations of the loaded salts are summarized in Table IV-1. The loaded concentrations of $NaHCO_3$ and Na_2CO_3 match with those in Excerpt IV-1.

Excerpt IV-1. Table 3-28 of Kirkes et al. (2014c).

Table 3-28 (continued) Preparation of experimental set-ups for the solubility of $PbCO_3$(s) in mixed Na_2CO_3 and $NaHCO_3$ solutions (the "$PbCl^+$—CO_3^{2-}" experiment).

Set-up ID	$PbCO_3$(s) (g)	$NaHCO_3$ (m)	Na2CO3(m)	Reference
PbCO3-Buffer A-1	2.0003	0.040	0.048	WIPP-Solubility-12 pg. 30
PbCO3-Buffer A-2	2.0012	0.040	0.048	WIPP-Solubility-12 pg. 30
PbCO3-Buffer B-1	2.0000	0.096	0.167	WIPP-Solubility-12 pg. 30
PbCO3-Buffer B-2	2.0007	0.096	0.167	WIPP-Solubility-12 pg. 30
PbCO3-Buffer C-1	2.0009	0.225	0.477	WIPP-Solubility-12 pg. 30
PbCO3-Buffer C-2	2.0006	0.225	0.477	WIPP-Solubility-12 pg. 30
PbCO3-Buffer D-1	2.0001	0.286	0.768	WIPP-Solubility-12 pg. 30
PbCO3-Buffer D-2	2.0001	0.286	0.768	WIPP-Solubility-12 pg. 30
PbCO3-Buffer E-1	2.0007	0.349	1.235	WIPP-Solubility-12 pg. 30
PbCO3-Buffer E-2	2.0008	0.349	1.235	WIPP-Solubility-12 pg. 30
PbCO3-Buffer F-1	2.0019	0.364	1.396	WIPP-Solubility-12 pg. 30
PbCO3-Buffer F-2	2.0000	0.364	1.396	WIPP-Solubility-12 pg. 30

Information Only

190 Excerpt IV-2. WIPP-Solubility-12, page 30.

30 PROJECT Fe-Pb-EDTA Solubility Notebook No. WIPP-Solubility-1:
Continued From Page

7/27/10

Mettler Toledo AT261 DeltaRange Balance and Mettler AE163 Dual-range balance both passed calibration checks. See Balance Calibration ~~Records~~ pg. 75.
Records-7 DAG 8/11/10

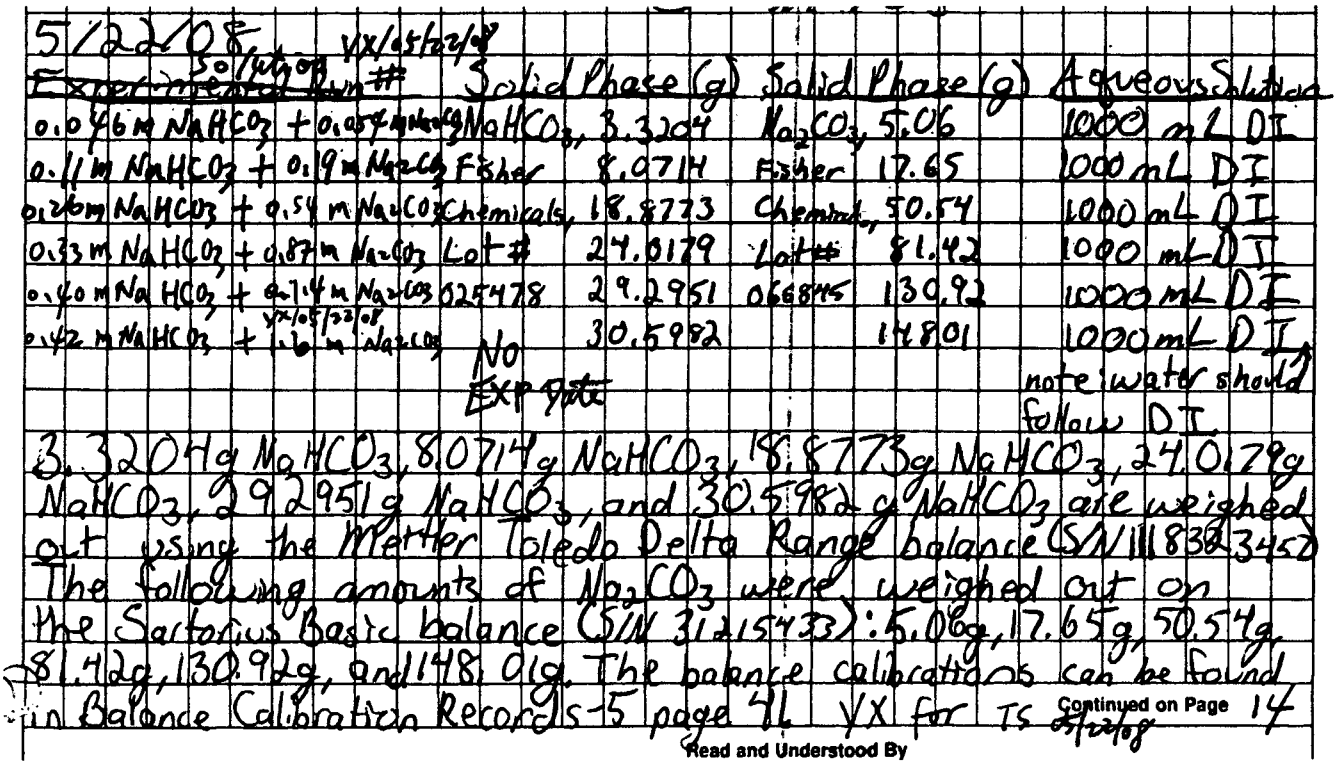
Today an experiment was set up using $PbCO_3$ as the solid phase. An aqueous solution of $NaHCO_3$ and Na_2CO_3 will also be used.

Experimental Run #	$PbCO_3$ (g)	Aqueous Solution (100mL)	Time Started
$PbCO_3$-BufferA-1	2.0003	0.046m $NaHCO_3$ + 0.054m Na_2CO_3	11:02 AM
$PbCO_3$-BufferA-2	2.0012	WIPP-Solubility-3 pg. 13 JK 11/18/10	11:07 AM
$PbCO_3$-BufferB-1	2.0000	0.11m $NaHCO_3$ + 0.19m Na_2CO_3	11:10 AM
$PbCO_3$-BufferB-2	2.0007	WIPP Solubility-3 pg. 13 JK 11/18/10	11:12 AM
$PbCO_3$-BufferC-1	2.0009	0.26m $NaHCO_3$ + 0.54m Na_2CO_3	11:15 PM
$PbCO_3$-BufferC-2	2.0006	WIPP Solubility-3 pg. 13 JK 11/18/10	11:16 AM
$PbCO_3$-Buffer-D-1	2.0001	0.33m $NaHCO_3$ + 0.87m Na_2CO_3	11:20 AM
$PbCO_3$-BuffD-2	2.0001	WIPP Solubility-3 pg. 13 JK 11/18/10	11:21 AM
$PbCO_3$-BufferE-1	2.0007	0.40m $NaHCO_3$ + 1.4m Na_2CO_3	11:24 AM
$PbCO_3$-BufferE-2	2.0008	WIPP Solubility-3 pg. 13 JK 11/18/10	11:25 AM
$PbCO_3$-BufferF-1	2.0019	0.42m $NaHCO_3$ + 1.58m Na_2CO_3	11:20 AM
$PbCO_3$-BufferF-2	2.0000	WIPP Solubility-3 pg. 13 JK 11/19/10	11:23 AM

191

Information Only

192 Excerpt IV-3. WIPP-Solubility-3, pages 13, 14.



5/22/08 YX/05/22/08

Experimental Run #	Solid Phase (g)	Solid Phase (g)	Aqueous Solution
0.046 m $NaHCO_3$ + 0.054 m Na_2CO_3	$NaHCO_3$, 3.3204	Na_2CO_3, 5.06	1000 mL DI
0.11 m $NaHCO_3$ + 0.19 m Na_2CO_3	Fisher 8.0714	Fisher 17.65	1000 mL DI
0.26 m $NaHCO_3$ + 0.54 m Na_2CO_3	Chemicals, 18.8773	Chemicals, 50.54	1000 mL DI
0.33 m $NaHCO_3$ + 0.87 m Na_2CO_3	Lot # 24.0179	Lot # 81.42	1000 mL DI
0.40 m $NaHCO_3$ + 1.4 m Na_2CO_3	025478 29.2951	066815 130.92	1000 mL DI
0.42 m $NaHCO_3$ + 1.6 m Na_2CO_3 YX/05/22/08	30.5982	148.01	1000 mL DI
	No Exp Data		note: water should follow DI

3.3204g $NaHCO_3$, 8.0714g $NaHCO_3$, 18.8773g $NaHCO_3$, 24.0179g $NaHCO_3$, 29.2951g $NaHCO_3$, and 30.5982g $NaHCO_3$ are weighed out using the Mettler Toledo Delta Range balance (S/N 1118383457). The following amounts of Na_2CO_3 were weighed out on the Sartorius Basic balance (S/N 31215433): 5.06g, 17.65g, 50.54g, 81.42g, 130.92g, and 148.01g. The balance calibrations can be found in Balance Calibration Records-5 page 41. YX for TS 05/22/08

Continued on Page 14

Read and Understood By

193

14 PROJECT Fe-Pb-EDTA SOLUBILITY Notebook No. WIPP-SOLUBILITY-3

Continued From Page 13

5/22/08

The following combinations of $NaHCO_3$ and Na_2CO_3 were mixed into 1000mL DI water with a stirrer: 3.3204g $NaHCO_3$ + 5.06g Na_2CO_3; 8.0714g $NaHCO_3$ + ~~50.54g~~ 17.65g Na_2CO_3; 18.8773g $NaHCO_3$ + ~~81.42g Na_2CO_3~~ + 50.54g Na_2CO_3; 24.0179g $NaHCO_3$ + 81.42g Na_2CO_3; 29.2951g $NaHCO_3$ + 130.92g Na_2CO_3; 30.5982g $NaHCO_3$ + 148.01g Na_2CO_3. The 1000mL DI water was measured using a 1000mL volumetric flask. TS 05/22/08 by YX/02/24/09

194

Information Only

Table IV-1. Recipe for aqueous solution used in the reactor preparation. The salt concentrations were verified by tracing back to Scientific Notebooks. 2.00 grams of $PbCO_3$(s) (cerussite; Formula weight = 267.21 g/mol) were added to the six solutions in duplicate, i.e., 12 reactors in total.

Reactor ID	NaHCO3, g	Na2CO3, g	DI, mL	DI, kg	Reference	NaHCO3, m	Na2CO3, m	ΣNa (m, Loading)	ΣCO3 (m, Loading)	M:m, L/kg
PbCO3-Buffer A-(1,2)	3.3204	5.06	1000	0.997	WS3/13,14	3.96E-02	4.79E-02	1.35E-01	8.75E-02	1.002
PbCO3-Buffer B-(1,2)	8.0714	17.65	1000	0.997	WS3/13,14	9.64E-02	1.67E-01	4.30E-01	2.63E-01	1.008
PbCO3-Buffer C-(1,2)	18.8773	50.54	1000	0.997	WS3/13,14	2.25E-01	4.78E-01	1.18E+00	7.04E-01	1.024
PbCO3-Buffer D-(1,2)	24.0179	81.42	1000	0.997	WS3/13,14	2.87E-01	7.71E-01	1.83E+00	1.06E+00	1.037
PbCO3-Buffer E-(1,2)	29.2951	130.92	1000	0.997	WS3/13,14	3.50E-01	1.24E+00	2.83E+00	1.59E+00	1.057
PbCO3-Buffer F-(1,2)	30.5982	148.01	1000	0.997	WS3/13,14	3.65E-01	1.40E+00	3.17E+00	1.77E+00	1.064

Reactor ID	NaHCO3, M	Na2CO3, M	ΣNa (M, Loading)	ΣCO3 (M, Loading)	Reaction volume, mL	ΣPb (M, Loading)	pH_{NIST}	pcH	A
PbCO3-Buffer A-(1,2)	3.96E-02	4.78E-02	1.35E-01	8.73E-02	100	7.48E-02	10.02	9.84	-0.18
PbCO3-Buffer B-(1,2)	9.56E-02	1.66E-01	4.27E-01	2.61E-01	100	7.48E-02	10.04	9.74	-0.29
PbCO3-Buffer C-(1,2)	2.20E-01	4.67E-01	1.15E+00	6.87E-01	100	7.48E-02	9.94	9.54	-0.40
PbCO3-Buffer D-(1,2)	2.76E-01	7.43E-01	1.76E+00	1.02E+00	100	7.48E-02	9.94	9.51	-0.43
PbCO3-Buffer E-(1,2)	3.31E-01	1.17E+00	2.68E+00	1.50E+00	100	7.48E-02	9.95	9.51	-0.44
PbCO3-Buffer F-(1,2)	3.43E-01	1.32E+00	2.98E+00	1.66E+00	100	7.48E-02	9.95	9.52	-0.43

V. Data - Aqueous

Solution chemistry measurements in this Section V are imported from Kirkes et al. (2014c). See individual subsections below for the identifiers of Tables in Kirkes et al. (2014c) where each component measurements are listed.

V.1. pHr

The temporal measurements of pHr are tabulated and displayed in Table V-1 and Figure V-1. No systematic change was observed as a function of time in the six experimental conditions. The observed data scatter is within 1% of precision as %2SD[5] (Table V-2). The change of the measured pHr as a function of ΣCO3 loading is displayed in Figure V-2. The averaged pHr are statistically identical at ~9.9. They show trend of decrease as the ΣCO3 loading lowers. The exception marked with green oval in Figure V-2 is discussed in Section VII. Observations.

[5] SD: Standard Deviation under normal distribution.

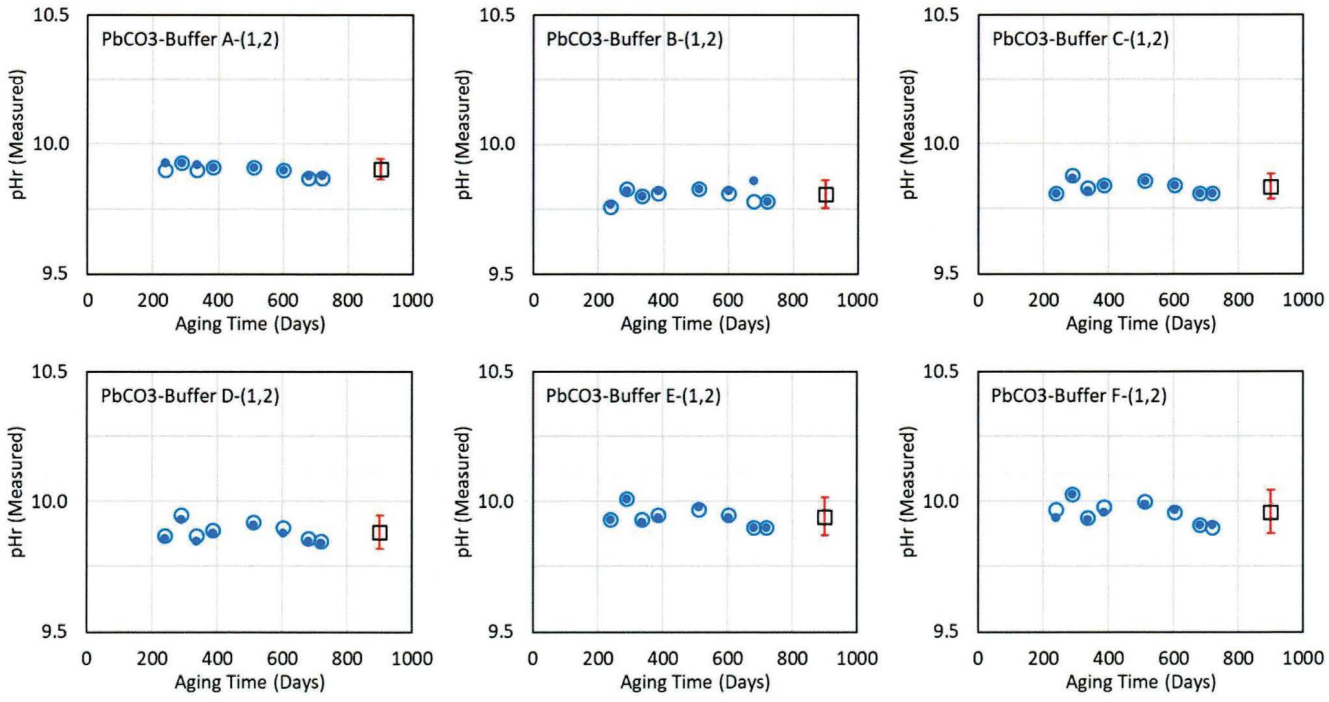
Information Only

Table V-1. Time-dependent measurements of pHr (Table 3-29 in page 99 of Kirkes et al. (2014c)).

pHr	DSP							
Reactor ID	238	287	336	385	511	601	679	720
PbCO3-Buffer A-1	9.93	9.93	9.92	9.91	9.91	9.90	9.88	9.88
PbCO3-Buffer A-2	9.90	9.93	9.90	9.91	9.91	9.90	9.87	9.87
PbCO3-Buffer B-1	9.77	9.82	9.80	9.82	9.83	9.82	9.86	9.78
PbCO3-Buffer B-2	9.76	9.83	9.80	9.81	9.83	9.81	9.78	9.78
PbCO3-Buffer C-1	9.81	9.87	9.82	9.84	9.86	9.84	9.81	9.81
PbCO3-Buffer C-2	9.81	9.88	9.83	9.84	9.86	9.84	9.81	9.81
PbCO3-Buffer D-1	9.86	9.93	9.85	9.88	9.91	9.88	9.85	9.84
PbCO3-Buffer D-2	9.87	9.95	9.87	9.89	9.92	9.90	9.86	9.85
PbCO3-Buffer E-1	9.93	10.01	9.92	9.94	9.98	9.94	9.90	9.90
PbCO3-Buffer E-2	9.93	10.01	9.93	9.95	9.97	9.95	9.90	9.90
PbCO3-Buffer F-1	9.94	10.03	9.93	9.96	9.99	9.97	9.91	9.91
PbCO3-Buffer F-2	9.97	10.03	9.94	9.98	10.00	9.96	9.91	9.90

DSP: Days Since Preparation = Aging time in days

Figure V-1. Plots of the time-dependent measurements of pHr. Dots and circles are measurements of duplicate reactors.



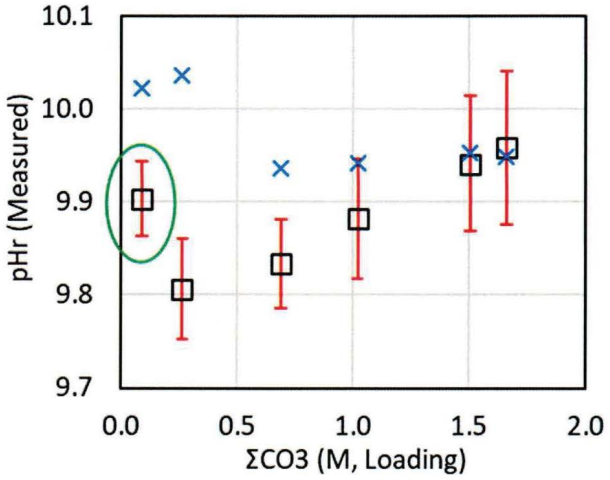
Information Only

218 Table V-2. Statistics of pHr measurements.

pHr				
Reactor ID	Average	2SD	%2SD	Count
PbCO3-Buffer A-(1,2)	9.90	0.04	0%	16
PbCO3-Buffer B-(1,2)	9.81	0.05	1%	16
PbCO3-Buffer C-(1,2)	9.83	0.05	0%	16
PbCO3-Buffer D-(1,2)	9.88	0.06	1%	16
PbCO3-Buffer E-(1,2)	9.94	0.07	1%	16
PbCO3-Buffer F-(1,2)	9.96	0.08	1%	16

219

220 Figure V-2. pHr measurements as a function of ΣCO3 loading. Blue cross symbols are
221 the pH calculated on the NIST scale for the solution prior to dissolving $PbCO_3$(s)
222 (cerussite). See Section VII for mass balance evaluation of H^+ and discussion of
223 the data point marked with green oval.



224

225 V.2. ΣPb

226 The temporal measurements of ΣPb are tabulated and plotted in Table V-3 and Figure V-3. The
227 measurements did not show systematic changes. The observed data scatter is within the
228 maximum %2SD of 11%, with one exception of 55% (Figure V-3, Table V-4). Change of the
229 averaged ΣPb as a function of ΣCO3 loading is presented in Figure V-4. ΣPb are less than 10^{-3} M, and
230 much lower than the $PbCO_3$(s) loading (0.075 M; Table IV-1). Therefore, more than 98% of the
231 loaded Pb as $PbCO_3$(s) resides in the solid phase. The two data points marked with red oval in Figure
232 V-3 are discussed in Section IX.2.

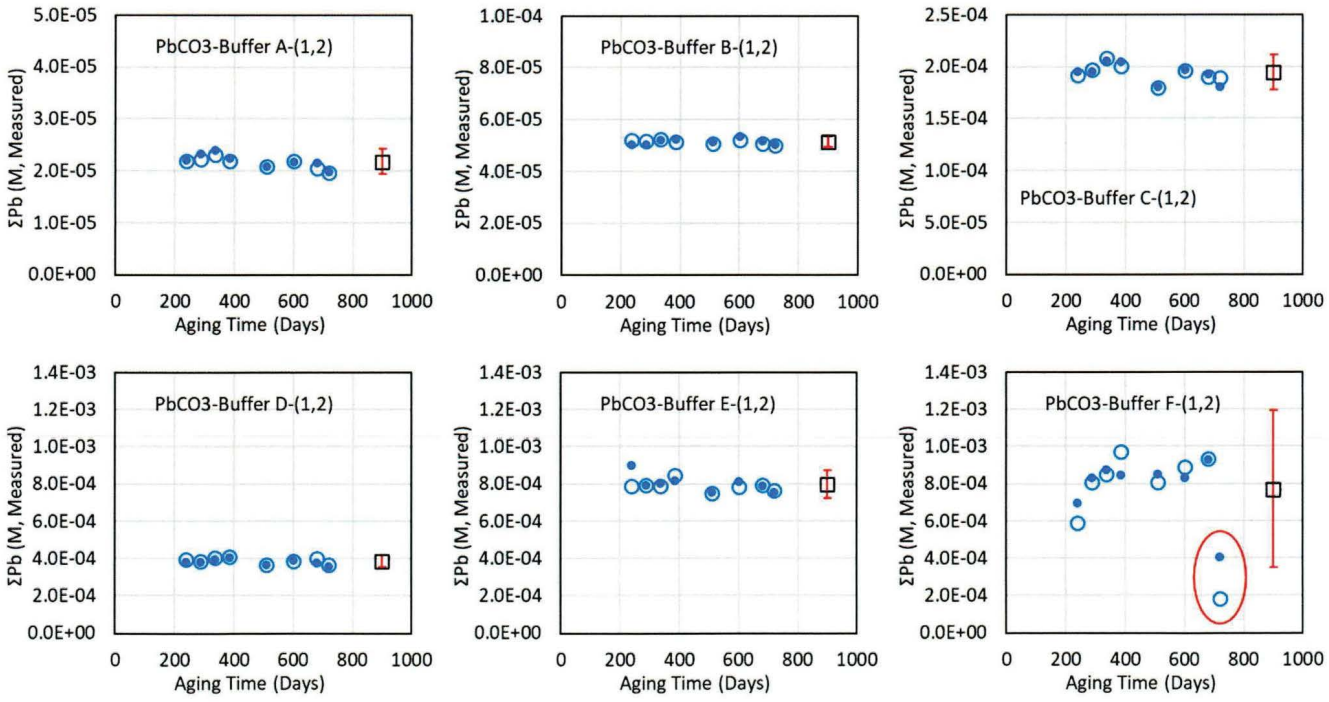
Information Only

Table V-3. Time-dependent measurements of ΣPb (Table 3-29 in page 101 of Kirkes et al. (2014c)).

ΣPb (M, Measured)	DSP							
Reactor ID	238	287	336	385	511	601	679	720
PbCO3-Buffer A-1	2.21E-05	2.33E-05	2.40E-05	2.24E-05	2.09E-05	2.17E-05	2.15E-05	1.98E-05
PbCO3-Buffer A-2	2.19E-05	2.23E-05	2.31E-05	2.20E-05	2.09E-05	2.20E-05	2.05E-05	1.96E-05
PbCO3-Buffer B-1	5.03E-05	5.05E-05	5.20E-05	5.24E-05	5.14E-05	5.36E-05	5.18E-05	5.03E-05
PbCO3-Buffer B-2	5.20E-05	5.19E-05	5.25E-05	5.14E-05	5.06E-05	5.21E-05	5.06E-05	5.01E-05
PbCO3-Buffer C-1	1.95E-04	1.95E-04	2.06E-04	2.05E-04	1.81E-04	1.97E-04	1.93E-04	1.81E-04
PbCO3-Buffer C-2	1.92E-04	1.97E-04	2.08E-04	2.01E-04	1.80E-04	1.96E-04	1.90E-04	1.89E-04
PbCO3-Buffer D-1	3.80E-04	3.82E-04	3.95E-04	4.05E-04	3.65E-04	3.92E-04	3.75E-04	3.55E-04
PbCO3-Buffer D-2	3.97E-04	3.88E-04	4.07E-04	4.08E-04	3.68E-04	3.84E-04	3.99E-04	3.66E-04
PbCO3-Buffer E-1	9.01E-04	7.94E-04	8.04E-04	8.20E-04	7.55E-04	8.13E-04	7.89E-04	7.55E-04
PbCO3-Buffer E-2	7.88E-04	7.94E-04	7.91E-04	8.46E-04	7.48E-04	7.86E-04	7.95E-04	7.64E-04
PbCO3-Buffer F-1	6.97E-04	8.33E-04	8.76E-04	8.46E-04	8.54E-04	8.33E-04	9.29E-04	4.07E-04
PbCO3-Buffer F-2	5.88E-04	8.07E-04	8.53E-04	9.73E-04	8.07E-04	8.90E-04	9.35E-04	1.84E-04

DSP: Days Since Preparation = Aging time in days

Figure V-3. Plots of time-dependent measurements of ΣPb. Dots and circles are measurements of duplicate reactors. See Section Section IX.2 to find explanation for the two data points marked with a red oval in the last panel.



Information Only

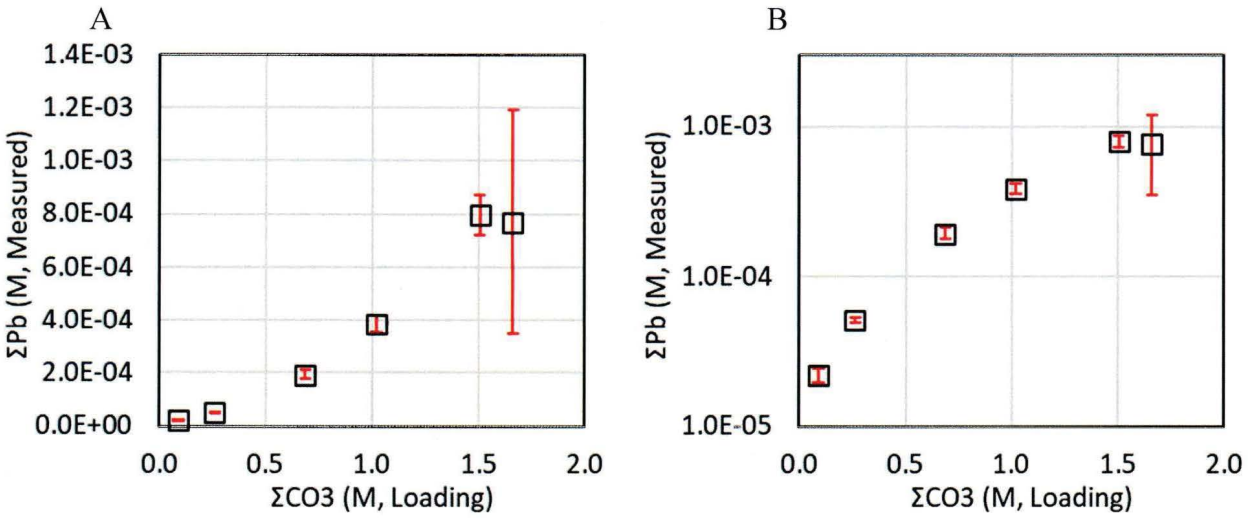
241 Table V-4. Statistics of ΣPb measurements.

ΣPb (M, Measured)				
Reactor ID	Average	2SD	%2SD	Count
PbCO3-Buffer A-(1,2)	2.18E-05	2.41E-06	11%	16
PbCO3-Buffer B-(1,2)	5.15E-05	1.99E-06	4%	16
PbCO3-Buffer C-(1,2)	1.94E-04	1.72E-05	9%	16
PbCO3-Buffer D-(1,2)	3.85E-04	3.26E-05	8%	16
PbCO3-Buffer E-(1,2)	7.96E-04	7.55E-05	9%	16
PbCO3-Buffer F-(1,2)	7.70E-04	4.21E-04	55%	16

242

243 Figure V-4. Change of ΣPb as a function of ΣCO3 loading. A. Linear scale. B. Log scale
244 to be compared with Excerpt IX-6 and Excerpt IX-7 in Section IX.2.

245



246

247 V.3. ΣCO3

248 The temporal measurements of ΣCO3 are tabulated and plotted in Table V-5 and Figure V-5. The
249 measurements did not show systematic changes with time. The observed data scatter is within the
250 maximum %2SD of 9%, and the %Deviation of the measured ΣCO3 from the loading were within the
251 precision of the measurements (Table V-6), reproducing the loaded concentrations. One exception is
252 marked in green italic font in Table V-6. The accuracy and precision of ΣCO3 measurements are
253 displayed in Figure V-6.

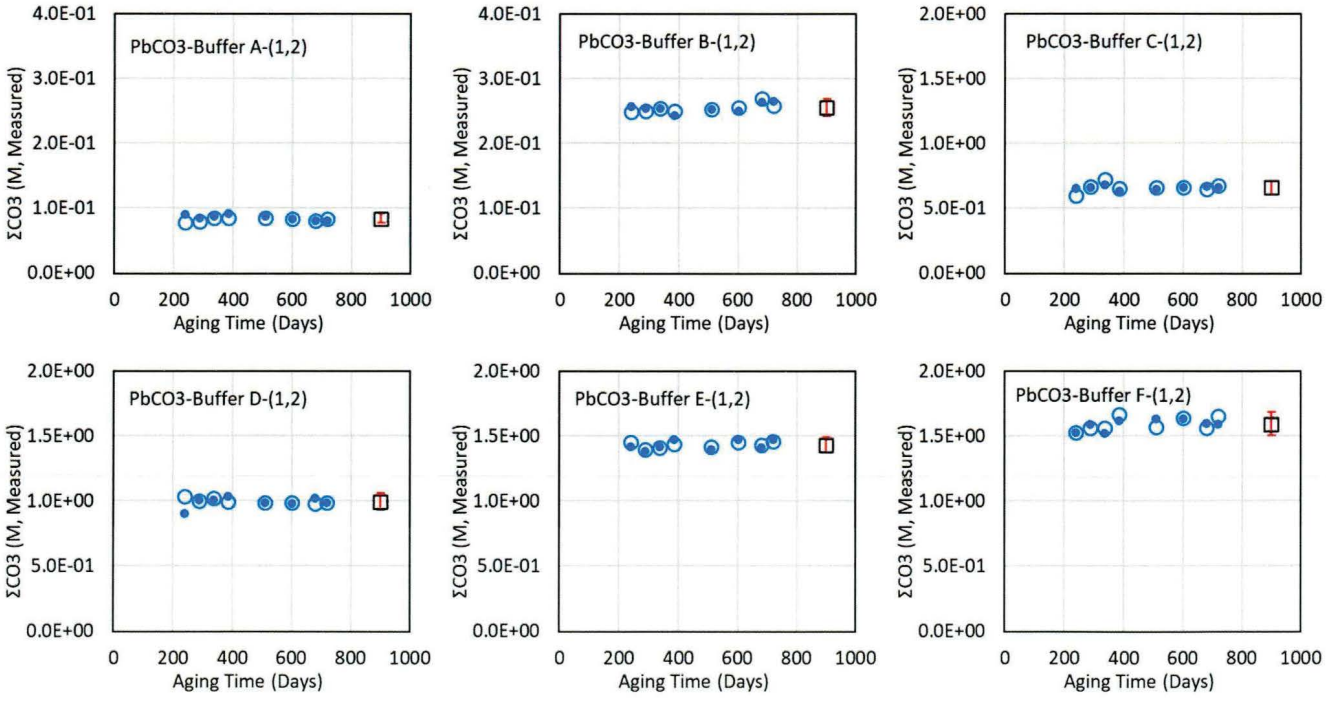
Information Only

Table V-5. Time-dependent measurements of ΣCO3 (Table 3-29 in page 103 of Kirkes et al. (2014c)).

ΣCO3 (M, Measured)	DSP							
Reactor ID	238	287	336	385	511	601	679	720
PbCO3-Buffer A-1	9.02E-02	8.53E-02	8.80E-02	9.28E-02	8.80E-02	8.33E-02	8.08E-02	8.12E-02
PbCO3-Buffer A-2	7.84E-02	8.03E-02	8.48E-02	8.59E-02	8.54E-02	8.38E-02	8.06E-02	8.42E-02
PbCO3-Buffer B-1	2.57E-01	2.54E-01	2.55E-01	2.44E-01	2.53E-01	2.50E-01	2.64E-01	2.65E-01
PbCO3-Buffer B-2	2.49E-01	2.50E-01	2.55E-01	2.50E-01	2.53E-01	2.56E-01	2.70E-01	2.58E-01
PbCO3-Buffer C-1	6.52E-01	6.60E-01	6.83E-01	6.33E-01	6.47E-01	6.60E-01	6.66E-01	6.64E-01
PbCO3-Buffer C-2	5.97E-01	6.68E-01	7.28E-01	6.55E-01	6.61E-01	6.62E-01	6.45E-01	6.75E-01
PbCO3-Buffer D-1	9.02E-01	1.01E+00	1.01E+00	1.04E+00	9.87E-01	9.80E-01	1.02E+00	9.91E-01
PbCO3-Buffer D-2	1.04E+00	1.00E+00	1.02E+00	9.93E-01	9.88E-01	9.90E-01	9.83E-01	9.91E-01
PbCO3-Buffer E-1	1.42E+00	1.38E+00	1.42E+00	1.47E+00	1.40E+00	1.47E+00	1.41E+00	1.47E+00
PbCO3-Buffer E-2	1.45E+00	1.40E+00	1.41E+00	1.44E+00	1.42E+00	1.45E+00	1.43E+00	1.46E+00
PbCO3-Buffer F-1	1.53E+00	1.59E+00	1.52E+00	1.62E+00	1.63E+00	1.63E+00	1.60E+00	1.59E+00
PbCO3-Buffer F-2	1.53E+00	1.56E+00	1.56E+00	1.67E+00	1.57E+00	1.64E+00	1.56E+00	1.65E+00

DSP: Days Since Preparation = Aging time in days

Figure V-5. Plots of the time-dependent measurements of ΣCO3. Dots and circles represent measurements of the duplicate reactors.

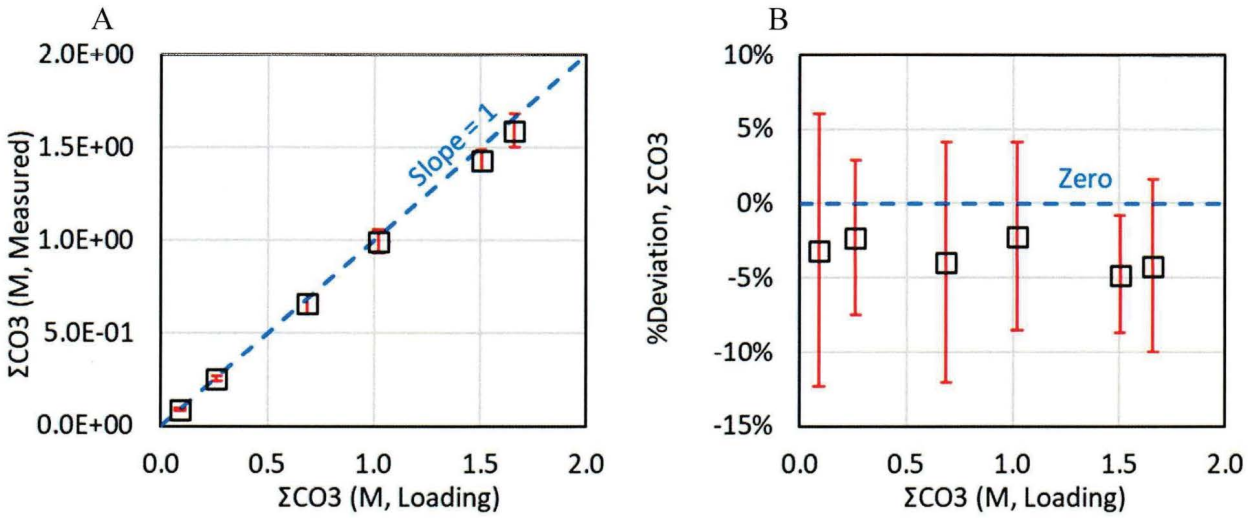


Information Only

Table V-6. Statistics of the measured ΣCO3.

ΣCO3 (M, Measured)					
Reactor ID	Average	2SD	%2SD	Count	%Dev
PbCO3-Buffer A-(1,2)	8.46E-02	7.76E-03	9%	16	-3%
PbCO3-Buffer B-(1,2)	2.55E-01	1.33E-02	5%	16	-2%
PbCO3-Buffer C-(1,2)	6.60E-01	5.34E-02	8%	16	-4%
PbCO3-Buffer D-(1,2)	9.97E-01	6.31E-02	6%	16	-2%
PbCO3-Buffer E-(1,2)	1.43E+00	5.65E-02	*4%*	*16*	*-5%*
PbCO3-Buffer F-(1,2)	1.59E+00	9.22E-02	6%	16	-4%

Figure V-6. Accuracy and precision of ΣCO3 measurements. A. Measured vs. loaded ΣCO3. B. %Deviation of the measured ΣCO3 from the loading.



V.4. ΣNa

The temporal measurements of ΣNa are tabulated and plotted in Table V-7 and Figure V-7. The measurements did not show systematic changes with time. The observed data scatter is within the maximum %2SD of 13% (Table V-8, Figure V-8). The %Deviations of the measured ΣNa from the loadings (Figure V-8B) show a trend of decrease as the loading of ΣNa (or equivalently ΣCO3) lowers. The exception marked with green oval in Figure V-8B is discussed in Section VII. Observations.

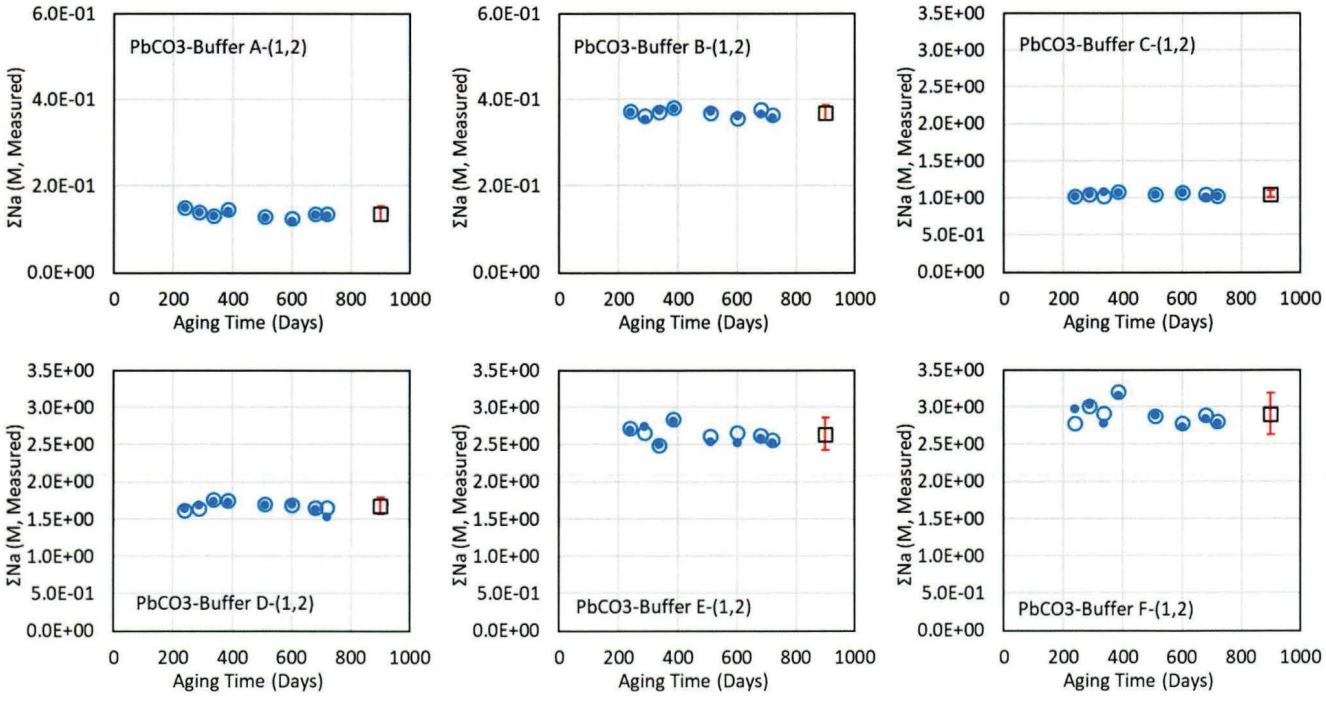
Information Only

Table V-7. Time-dependent measurements of ΣNa (Table 3-29 in page 100 of Kirkes et al. (2014c)).

ΣNa (M, Measured)	DSP							
Reactor ID	238	287	336	385	511	601	679	720
PbCO3-Buffer A-1	1.51E-01	1.41E-01	1.33E-01	1.42E-01	1.29E-01	1.20E-01	1.34E-01	1.33E-01
PbCO3-Buffer A-2	1.50E-01	1.41E-01	1.32E-01	1.46E-01	1.30E-01	1.25E-01	1.36E-01	1.36E-01
PbCO3-Buffer B-1	3.71E-01	3.55E-01	3.75E-01	3.80E-01	3.74E-01	3.63E-01	3.68E-01	3.59E-01
PbCO3-Buffer B-2	3.73E-01	3.63E-01	3.71E-01	3.82E-01	3.69E-01	3.57E-01	3.77E-01	3.65E-01
PbCO3-Buffer C-1	1.02E+00	1.06E+00	1.09E+00	1.08E+00	1.05E+00	1.08E+00	1.01E+00	1.03E+00
PbCO3-Buffer C-2	1.03E+00	1.05E+00	1.03E+00	1.09E+00	1.05E+00	1.08E+00	1.05E+00	1.03E+00
PbCO3-Buffer D-1	1.64E+00	1.69E+00	1.74E+00	1.73E+00	1.69E+00	1.71E+00	1.63E+00	1.54E+00
PbCO3-Buffer D-2	1.62E+00	1.65E+00	1.76E+00	1.75E+00	1.71E+00	1.69E+00	1.66E+00	1.66E+00
PbCO3-Buffer E-1	2.70E+00	2.75E+00	2.51E+00	2.82E+00	2.54E+00	2.53E+00	2.59E+00	2.53E+00
PbCO3-Buffer E-2	2.72E+00	2.66E+00	2.49E+00	2.85E+00	2.61E+00	2.66E+00	2.63E+00	2.57E+00
PbCO3-Buffer F-1	2.98E+00	3.04E+00	2.79E+00	3.16E+00	2.89E+00	2.73E+00	2.85E+00	2.78E+00
PbCO3-Buffer F-2	2.78E+00	3.02E+00	2.92E+00	3.21E+00	2.88E+00	2.79E+00	2.89E+00	2.81E+00

DSP: Days Since Preparation = Aging time in days

Figure V-7. Plots of the time-dependent measurements of ΣNa. Dots and circles are measurements of duplicate reactors.

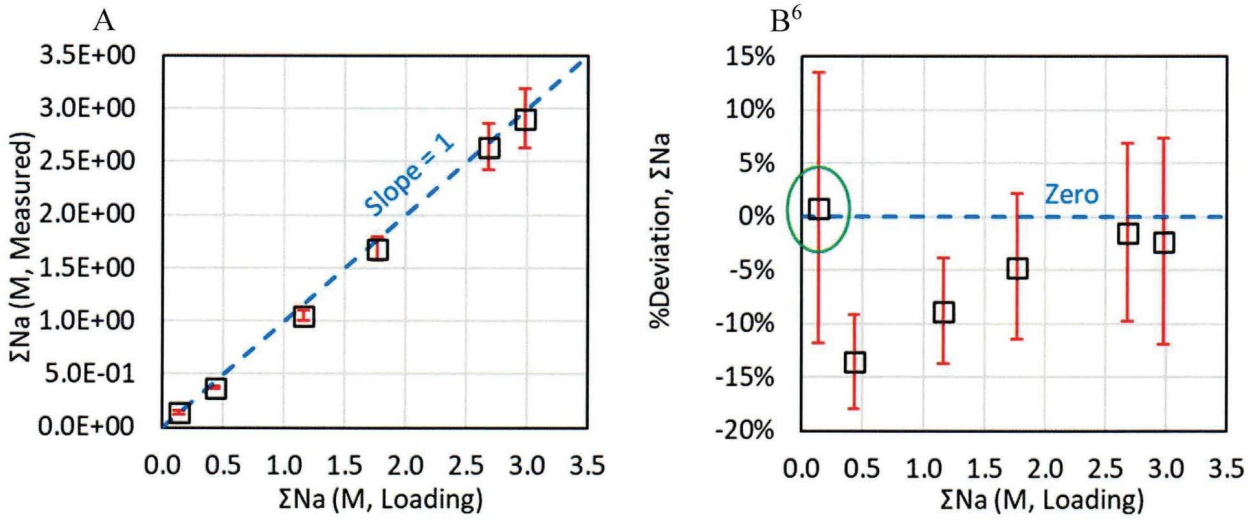


Information Only

Table V-8. Statistics of the measured ΣNa.

ΣNa (M, Measured)						
Reactor ID	Average	2SD	%2SD	Count	Dev	%Dev
PbCO3-Buffer A-(1,2)	1.36E-01	1.72E-02	13%	16	1.06E-03	1%
PbCO3-Buffer B-(1,2)	3.69E-01	1.61E-02	4%	16	-5.80E-02	-14%
PbCO3-Buffer C-(1,2)	1.05E+00	5.18E-02	5%	16	-1.02E-01	-9%
PbCO3-Buffer D-(1,2)	1.68E+00	1.14E-01	7%	16	-8.28E-02	-5%
PbCO3-Buffer E-(1,2)	2.64E+00	2.20E-01	8%	16	-4.04E-02	-2%
PbCO3-Buffer F-(1,2)	2.91E+00	2.81E-01	10%	16	-6.98E-02	-2%

Figure V-8. Accuracy and precision of ΣNa measurements. A. Measured vs. loaded ΣNa. B. %Deviation of the measured ΣNa from the loading. See the mass balance discussion in Section VII. Observations for the data marked with green oval in B.



VI. Data - Solids

$PbCO_3$(s) (cerussite) and $NaPb_2(CO_3)_2(OH)$(s) (abellaite) co-exist at the lowest ΣCO3 loading. At higher ΣCO3 loadings, X-ray diffraction (XRD) peaks of cerussite disappeared (Excerpt VI-1, Excerpt VI-2, Figure VI-1).

[6] LDL issue similar to the observation made from $PbCO_3$(s) - Na_2CO_3 - NaCl - H_2O where the formation of abellaite is also observed.

Information Only

Excerpt VI-1. Figures 27 to 32 in pages 36 to 38 of Kirkes and Xiong (2019). Formation of abellaite is reported.

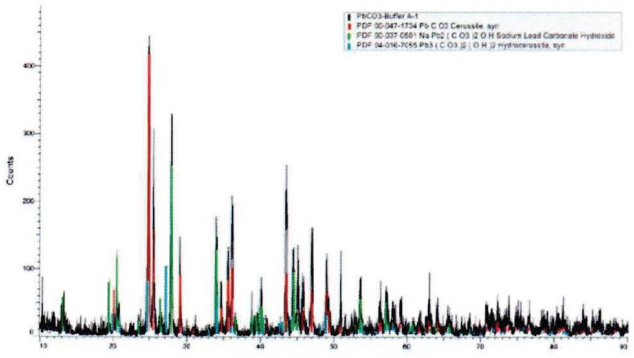


Figure 27 XRD pattern for sample PbCO3-Buffer A-1-Tentative ID
Source of Figure: WIPP-Solubility-50 Pg. 59

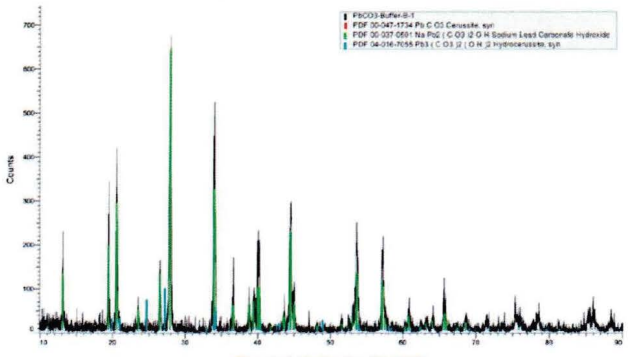


Figure 28 XRD pattern for sample PbCO3-Buffer B-1-Tentative ID
Source of Figure: WIPP-Solubility-50 Pg. 58

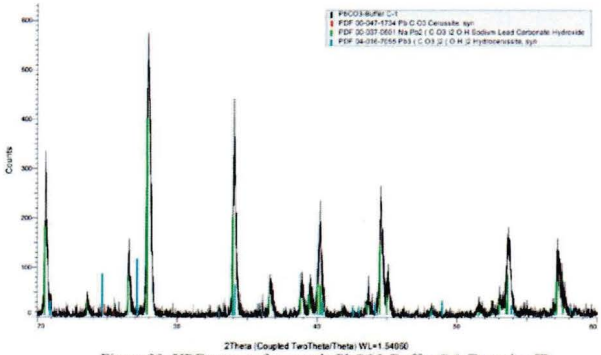


Figure 29 XRD pattern for sample PbCO3-Buffer C-1-Tentative ID
NOTE: This sample was ran from only 20° to 60° theta. The other samples in the set were analyzed from 10-90° theta.
Source of Figure: WIPP-Solubility-50 Pg. 59

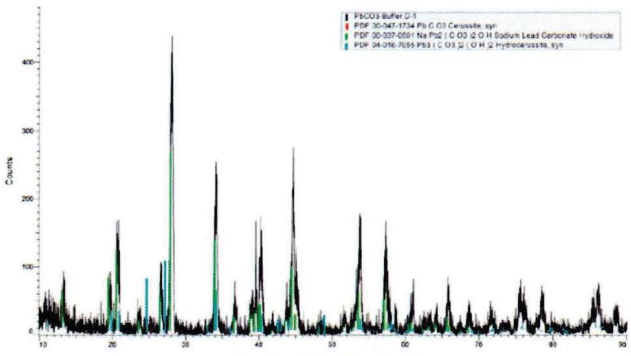


Figure 30 XRD pattern for sample PbCO3-Buffer D-1-Tentative ID
Source of Figure: WIPP-Solubility-50 Pg. 59

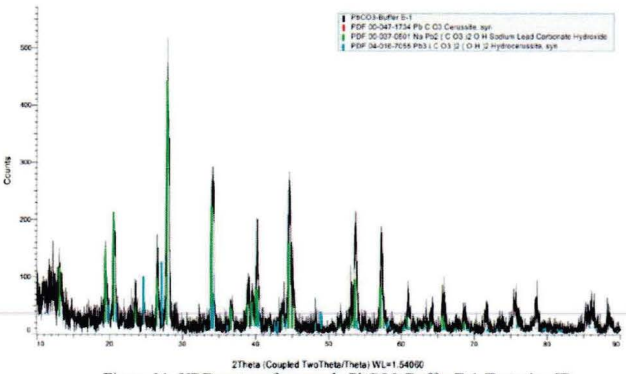


Figure 31 XRD pattern for sample PbCO3-Buffer E-1-Tentative ID
Source of Figure: WIPP-Solubility-50 Pg. 59

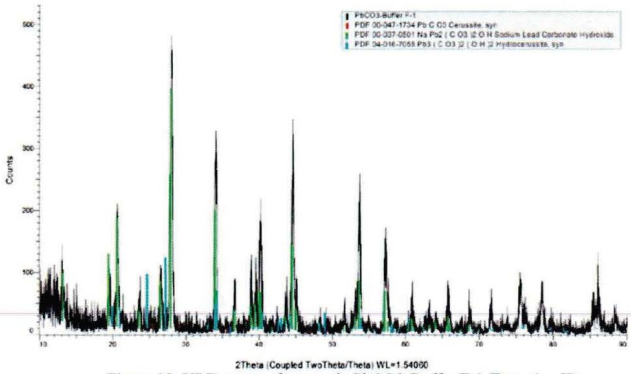


Figure 32 XRD pattern for sample PbCO3-Buffer F-1-Tentative ID
Source of Figure: WIPP-Solubility-50 Pg. 59

Information Only

296 Excerpt VI-2. Additional scans of solids collected from the reactors PbCO3-Buffer-D-1
297 and -2. Figures 33 and 34 in page 39 of Kirkes and Xiong(2019). Formation of
298 abellaite is reported therein.

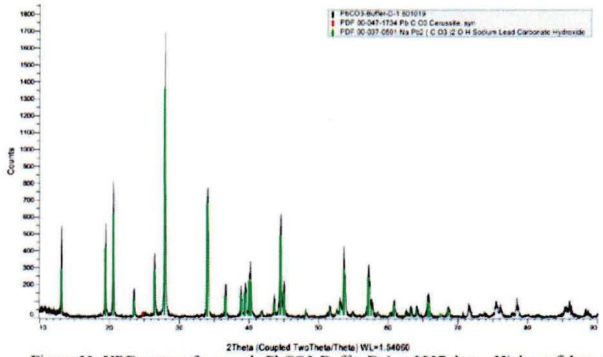


Figure 33 XRD pattern for sample PbCO3-Buffer D-1 at 3237 days. -High confidence ID
Source of Figure: WIPP-Solubility-49 Pg. 46

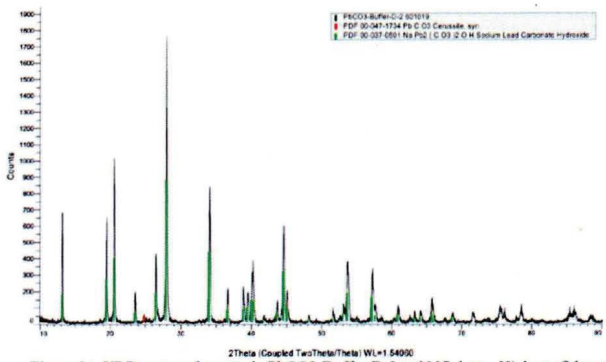
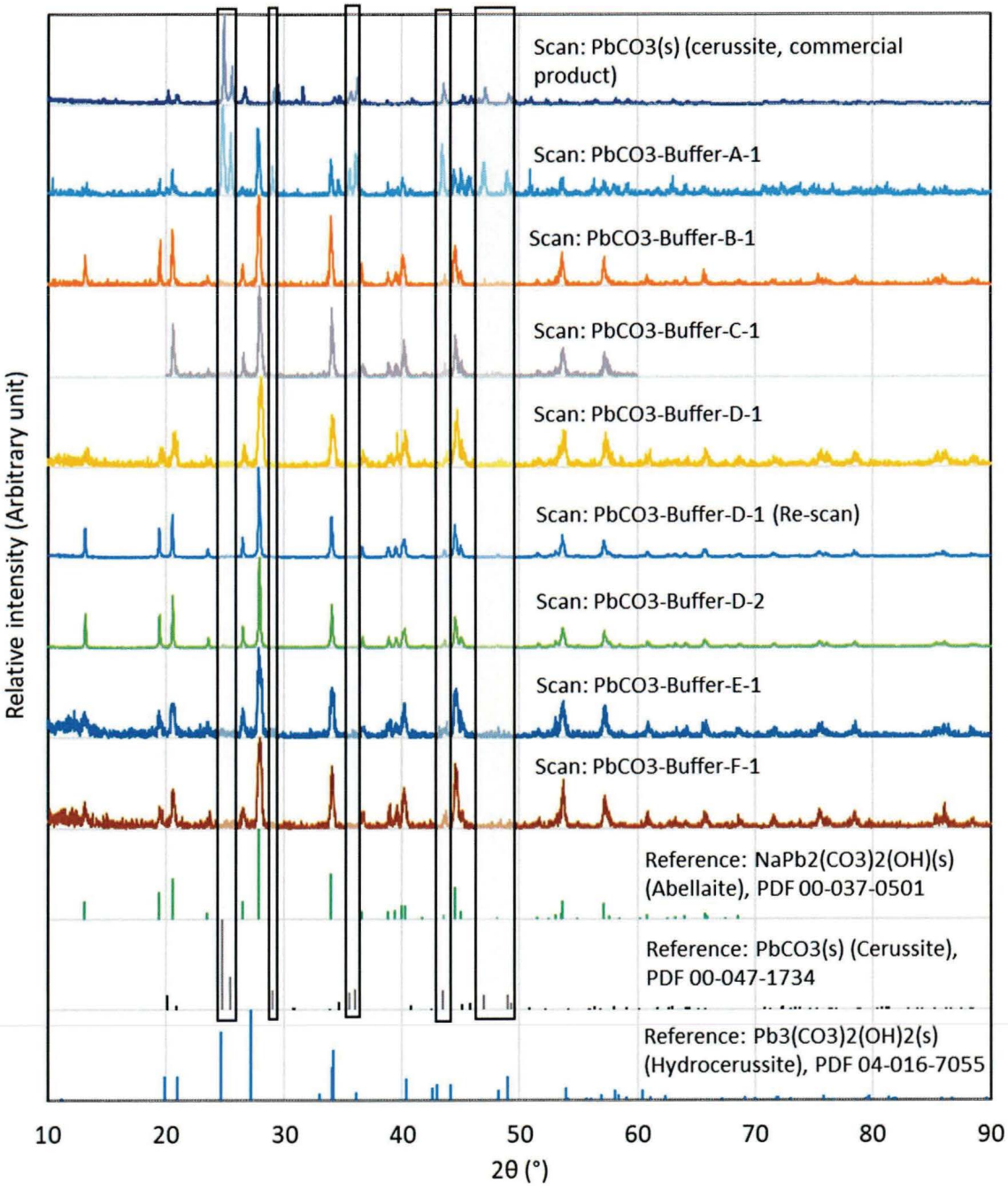


Figure 34 XRD pattern for sample PbCO3-Buffer-D-2 at 3237 days. -High confidence ID
Source of Figure: WIPP-Solubility-49 Pg. 46

299

Information Only

Figure VI-1. Re-plots of the XRD scans in Excerpt VI-1 and Excerpt VI-2. The elongated rectangles with gray tone indicate the locations of major reference peaks of $PbCO_3$(s) (cerussite).



VII. Observations

No systematic changes were observed in the time-dependent measurements of all system components. The measurements showed that data scatters within the calculated precisions, i.e., 2SD. Equilibrium attainment can be assumed.

Information Only

The averaged pHr show a trend between 9.7 and 10.0 (Figure V-2). The pHr is an approximation to the pH calculated on the NIST scale, since the commercial pH buffers used to calibrate the pH meter and electrode are formulated by the NIST definition of pH. When compared with the pH calculated on the NIST scale for the solutions without $PbCO_3$(s) (The values in Table IV-1 are displayed as blue crosses in Figure V-2), the trend of pHr suggests that at lower ΣCO3 loadings the change of pHr is more sensitive to the unit H^+ generated through Reaction (1) due to lower buffer capacity, i.e., lower concentrations of the $NaHCO_3$ and Na_2CO_3. Reaction (1) would be driven to the right by the chemical potential exerted by Na^+ and H_2O onto the added $PbCO_3$(s) (cerussite) (Le Chatelier's principle), and one of the products is H^+.

$$2PbCO_3(s)\ (Cerussite) + Na^+ + H_2O = NaPb_2(CO_3)_2(OH)(s)\ (Abellaite) + H^+ \quad (1)$$

The larger pHr value at the lowest loading of ΣCO3 (data in green oval in Figure V-2) can be interpreted as the following: The progress of Reaction (1) to the right is limited by Na^+. That is, at the lowest loading of ΣCO3, the loading of ΣNa is also at the lowest concentration (see Table IV-1).

2.00 grams of $PbCO_3$(s) (cerussite, formula weight = 267.21 g/mol) were added to 100 mL of solutions (Table IV-1). The added $PbCO_3$(s) is the sole source of Pb for both solid and aqueous phases. That is, 2.00 / 267.21 / 0.1 = 0.07484 ≡ 0.075 M of Pb is distributed in solid and aqueous phases. Dissolved Pb is less than 10^{-3} M (ΣPb in Table V-4), so more than 98% of 0.075 M Pb added in the form of $PbCO_3$(s) (i.e., > 0.073 M) resides in the solid phase.

XRD scans (Figure VI-1) indicated that cerussite-to-abellaite conversion is complete except at the lowest loading of ΣCO3 and ΣNa (scan: PbCO3-Buffer-A-1). By allowing 10% of the low detection limit of XRD for the existence of possibly remaining cerussite (but not resolved by XRD), more than 0.066 M of Pb added as $PbCO_3$(s) (cerussite) is now in the secondary mineral, i.e., 0.033 M of $NaPb_2(CO_3)_2(OH)$(s) (abellaite). For the formation of 0.033 M of abellaite, 0.033 M of Na^+ is taken from the solution (Reaction (1) in page 22). 0.033 M is the minimum removal of Na^+ from the solution to explain the mass balance, given the maximum dissolved Pb (10^{-3} M) and the detection limit of XRD (10%).

The removal of Na^+ from the solutions was 0.07 ± 0.05 M, which is |average|[7] and 2SD of the negative deviation (Dev) values in Table V-8. This 95% confidence interval (i.e., 0.02 to 0.12 M) is inclusive of the minimun value of 0.033 M Na^+ removed. The %Deviation is more negative at lower loadings of

[7] | | denotes the absolute value.

Information Only

ΣNa and ΣCO3 due to the constant removal of Na^+ (-0.07 ± 0.05 M), with an exception observed at the lowest loading of ΣNa (Figure V-8B).

Partial cerussite-to-abellaite conversion was observed at the lowest loading of ΣNa (or ΣCO3) (XRD in Figure VI-1). The large pHr value at the lowest ΣNa loading corroborates the partial conversion via Reaction (1) (data point marked with green oval in Figure V-2). The partial conversion indicates the depletion of the reactant, Na^+, due to the lowest ΣNa loading. However, a full recovery of ΣNa was observed as showed by the data point marked with a green oval in Figure V-8B.

If 30 to 60% of the conversion is assumed based on the XRD at the lowest loading of ΣNa, then 0.011 to 0.022 M Na^+ is to be removed[8] from solution and resides in the secondary mineral abellaite. The decrease of ΣNa in solution ranging 0.011 to 0.022 M would have been registered in the %Deviation ranging -8 to -16% from the loaded ΣNa (0.135 M; Table IV-1). Thus, it is unclear why the conspicuous full recovery of ΣNa was observed at the lowest ΣNa loading (Figure V-8B).[9]

If the full recovery is real at equilibrium, then the equilibrium solution composition at the lowest Na loading would place the stability boundary between $PbCO_3$(s) (cerussite) and $NaPb_2(CO_3)_2(OH)$(s) (abellaite). If the full recovery is an overestimation, cerussite is metastable relative to abellaite and would be expected to convert to abellaite upon addition of Na^+. Both cases suggest that now the abellaite is the solubility-limiting phase in the experiment at the lowest loading of ΣNa, just like other experiments in the remaining five solutions with higher ΣNa loadings.

The averaged ΣPb increases as the ΣCO3 loading increases (Figure V-4), which is indicative of the Pb^{+2} - CO_3^{-2} complexation. If Pb^{+2} is the sole lead dissolved species, the following reactions would have been driven to the left upon increase of the common-ion CO_3^{-2} according to Le Chatelier's principle, therefore suppressing the $\Sigma Pb \equiv [Pb^{+2}]$.

$$PbCO_3(s)\ (Cerussite) = Pb^{+2} + CO_3^{-2} \quad (2)$$

$$NaPb_2(CO_3)_2(OH)(s)\ (Abellaite) = 2Pb^{+2} + 2CO_3^{-2} + Na^+ + OH^- \quad (3)$$

Having identified the effect of the Pb^{+2} - CO_3^{-2} complexation, the ionic interaction of species pair Pb^{+2}/CO_3^{-2} may not need to be considered because the chemical affinity of Pb^{+2} and CO_3^{-2} can be

[8] (0.073 × 0.3 to 0.6 = 0.022 to 0.044) / 2 = 0.011 to 0.022 M.

[9] Possible explanations: contamination in DI water with low level of Na, inaccuracy of dilution exceeding 300 times, or low detection limit of ICP-AES (i.e., the precision is lowest at 13%, Table V-8). The samples injected to ICP-AES were diluted by more than 300 times, and the instrument readings were around 10 ppm Na. 10 × 300 / 22.99 / 1000 = 0.13 M Na. SNL WIPP Geochemistry would have to eliminate the possible explanations one-by-one as it established the accuracy and precision of analytical instruments, including ICP-AES.

Information Only

delineated as cumulative complexation,[10] and the concentration of the species Pb^{+2} ($[Pb^{+2}]$) would be too low to generate the signal of ionic interaction with one (or more) of the background ion(s) under the cumulative complexation construct, and such interaction would have little to no effect on the activity coefficient of the dominant Pb^{+2} - CO_3^{-2} complexes.

The measurements of ΣCO3 showed acceptable accuracy and precision. Consistent negative %Deviation was observed, while the |%Deviation| did not exceed 5%, and the precision as %2SD was less than 9% (Table V-6, Figure V-6). Per Reaction (1) in page 22, the cerussite-to-abellaite conversion is independent of the ΣCO3 loading, which could be one of the reasons for the full recovery within the analytical precision (Figure V-6).

The CO_2(g) loss reported in Table III.2-10 and Figure III.2-9 of GEOC-21-03 (Jang et al., 2021a) was larger than the loss of the experiments of this memo. The %Deviation reached down to -26%. The experiments reported in GEOC-21-03 were prepared at lower pH where the range of partial pressure of CO_2(g), denoted $P_{CO2(g)}$ hereafter, in the solutions ranged from $10^{-3.1}$ to $10^{-0.3}$ atm. The experiments being analyzed in this memo were conducted in solutions where the $P_{CO2(g)}$ ranged $10^{-3.8}$ to $10^{-3.0}$ atm. The atmospheric $P_{CO2(g)} = 10^{-3.5}$ atm (Stumm and Morgan, 1996). Thus, some of the reactors could have experienced ΣCO3 gain if they were open to the atmosphere for repeated sampling. Overall, $P_{CO2(g)}$ closer to atmospheric values could be another reason for the better recovery, i.e., less loss or gain of ΣCO3. Small negative %Deviation in Table V-6 and Figure V-6 could be attributed to the loss of CO_2(g) via filtration due to the adiabatic compression and expansion of dissolved CO_2(g).

VIII. Model Parameterization: Pitzer Approach

VIII.1. Molarity-to-molality Conversion

The concentrations in Molarity and the pHr presented in Section V were converted to molality (Table VIII-1) using the M:m values in Table IV-1.

$$m = M \times M{:}m \tag{4}$$

where m is molality (mol/kg) and M is Molarity (mol/L).

Conversion of pHr to pmH requires one more step. The A values to convert pHr to pcH were determined by the difference of pH_{NIST} and pcH calculated for the background solutions using EQ3NR (Table IV-1). The following equation was used.

[10] Cumulative complexation means the formation of $PbHCO_3^+$, $PbCO_3$(aq), $Pb(CO_3)_2^{-2}$, etc., as the loading of ΣCO3 increases.

Information Only

$$A = pcH_{calc} - pH_{NIST} \quad (5)$$

$$pcH = pHr + A \quad (6)$$

$$pmH = pcH - \log (M:m) \quad (7)$$

Table VIII-1. molalities of the system components.

Reactor ID	pcH	pmH		ΣPb		ΣCO3		ΣNa	
		Average	2SD	Average	2SD	Average	2SD	Average	2SD
PbCO3-Buffer A-(1,2)	9.72	9.72	0.04	2.18E-05	2.42E-06	8.47E-02	7.78E-03	1.36E-01	1.72E-02
PbCO3-Buffer B-(1,2)	9.51	9.51	0.05	5.19E-05	2.00E-06	2.57E-01	1.34E-02	3.72E-01	1.62E-02
PbCO3-Buffer C-(1,2)	9.44	9.43	0.05	1.99E-04	1.76E-05	6.76E-01	5.47E-02	1.08E+00	5.30E-02
PbCO3-Buffer D-(1,2)	9.45	9.43	0.06	4.00E-04	3.38E-05	1.03E+00	6.54E-02	1.74E+00	1.18E-01
PbCO3-Buffer E-(1,2)	9.50	9.48	0.07	8.42E-04	7.98E-05	1.51E+00	5.97E-02	2.78E+00	2.32E-01
PbCO3-Buffer F-(1,2)	9.53	9.50	0.08	8.18E-04	4.47E-04	1.69E+00	9.81E-02	3.09E+00	2.99E-01

VIII.2. Synthesis of a Thermodynamic Database

Thermodynamic quantities, i.e., log Ks and PIPs, for the four of the five system components (Na^+, HCO_3^-, H^+, and OH^-)[11] are imported from Harvie et al. (1984).

The reactions to delineate the ΣPb are imported from Powell et al. (2009), and listed in Table VIII-2. The log Ks in Table VIII-2 were scaled to I = 0 using SIT activity model (Powell et al., 2009). It is recommended to implement the log Ks in the speciation calculation in combination with the SIT parameters, i.e., the ε's. The ε's are the counterpart of PIPs in the SIT activity model.

As such, after implementing the SIT-log Ks into the PACE-based speciation calculation of this memo, the need of PIPs to support the SIT-based log Ks (Table VIII-2) will be gauged considering the uncertainty associated with the given experimental data (2SDs in Table VIII-1).

XRD indicates the formation of $NaPb_2(CO_3)_2(OH)$(s) (abellaite) in the six experimental conditions (Excerpt VI-1; Excerpt VI-2; Figure VI-1). So far, the log K for the dissolution of abellaite, Reaction (8), has not been located in the literature.

$$NaPb_2(CO_3)_2(OH)(s)\ (Abellaite) + 3H^+ = Na^+ + 2Pb^{+2} + 2HCO_3^- + H_2O \quad (8)$$

[11] $OH^- = H_2O - H^+$

Information Only

411 Table VIII-2. Reactions and the log Ks imported from Powell et al. (2009).

Reactions	Log K	Remarks
Aqueous Complexation		
$PbHCO_3^+ = Pb^{+2} + HCO_3^-$	-1.86 ± 0.1	Provisional (p.2429)
$Pb^{+2} + HCO_3^- = PbHCO_3^+$	1.86 ± 0.1	-1.86
$PbCO_3(aq) + H^+ = Pb^{+2} + HCO_3^-$	3.88 ± 0.72	Indicative (p.2429)
$Pb^{+2} + CO_3^{-2} = PbCO_3(aq)$	6.45 ± 0.72	-6.45 + 10.33 = 3.88
$Pb(CO_3)_2^{-2} + 2H^+ = Pb^{+2} + 2HCO_3^-$	10.53 ± 0.24	Provisional (p.2429)
$Pb^{+2} + 2CO_3^{-2} = Pb(CO_3)_2^{-2}$	10.13 ± 0.24	-10.13 + 2 × 10.33 = 10.53
$Pb(CO_3)OH^- + 2H^+ = Pb^{+2} + HCO_3^- + H_2O$	13.42 ± 0.2	Statistically predicted (p.2441)
$Pb^{+2} + CO_3^{-2} + OH^- = Pb(CO_3)OH^-$	10.9 ± 0.2	-10.9 + 10.33 + 13.99 = 13.42
Dissolution		
$PbCO_3(s)$ (Cerussite) $+ H^+ = Pb^{+2} + HCO_3^-$	-2.85 ± 0.07	Recommended (p.2429)
$PbCO_3(s)$ (Cerussite) $= Pb^{+2} + CO_3^{-2}$	-13.18 ± 0.07	-13.18 + 10.33 = -2.85

412 Texts in gray fonts: They are as listed in Powell et al. (2009). They should be converted to EQ3/6 database format as those in
413 black fonts.

414

415 ## VIII.3. Assessment of the Solubility Limiting Phase(s)

416 Using the molalities in Table VIII-1, six EQ3NR input files (*.3i) were prepared.[12] They were
417 executed through EQ3NR to calculate the saturation index (SI) and aqueous speciation. Five reactions
418 and their SIT-based log Ks in Table VIII-2 were used in the calculation (Figure VIII-1).

419 The calculation indicates that the initial solid, $PbCO_3(s)$ (cerussite), is undersaturated (i.e., negative SIs
420 in Figure VIII-1A). The major dissolved Pb species is $Pb(CO_3)_2^{-2}$. The less negative SI of cerussite
421 marked with red rectangle in Figure VIII-1A is consistent with the uncertainty associated with the ΣNa
422 measurements (see discussion in Section VII). By the log K of $2PbCO_3.Pb(OH)_2(s)$ (hydrocerussite)
423 defined in Edwards et al. (1992) and Bilinski and Schinder (1982), it showed undersaturation.

424 The quotient of component activities, Q, that consist of $NaPb_2(CO_3)_2(OH)(s)$ (abellaite) can be
425 calculated using the activities of components of Reaction (8) as in Equation (9). The log component
426 activities, denoted "log {component}" hereafter, and the calculated log Qs for the six experimental
427 conditions are listed in Table VIII-3.

428 $$\text{Log Q (Abellaite)} = -3\cdot\log\{H^+\} + \log\{Na^+\} + 2\cdot\log\{Pb^{+2}\} + 2\cdot\log\{HCO_3^-\} + \log\{H_2O\}$$

429 $$= 2.77 \pm 0.62 \qquad (9)$$

[12] The files to be archived in the following link: (CVS/CVSLIB/WIPP EXTERNAL/ap190)

Information Only

Figure VIII-1. A. Saturation index of $PbCO_3$(s) (cerussite). B. Major species in action is $Pb(CO_3)_2^{-2}$.

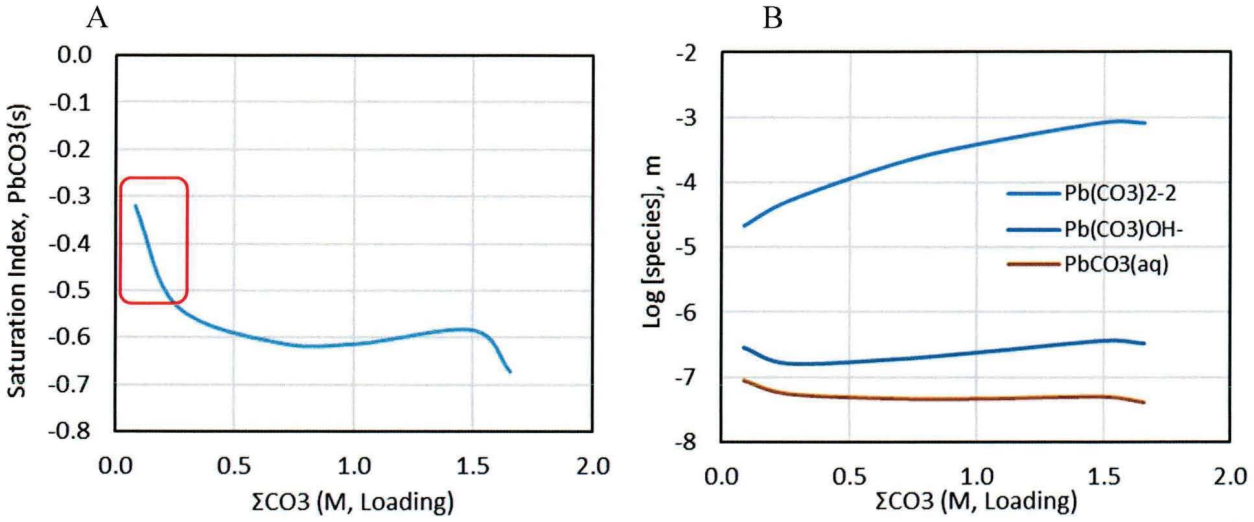


Table VIII-3. Log activities of components (log {component}) consisting of the dissolution of $NaPb_2(CO_3)_2(OH)$(s) (abellaite), i.e., Equation (9). The log quotient (log Q) of the log activities of the components by Equation (9) are calculated and listed in the last column.

Log $\{Na^+\}$	Log $\{HCO_3^-\}$	Log $\{H^+\}$	Log $\{Pb^{+2}\}$	Log $\{H_2O\}$	Log Q
-1.00	-1.51	-9.88	-11.54	0.00	2.54
-0.61	-1.14	-9.75	-11.99	0.00	2.37
-0.19	-0.96	-9.76	-12.26	-0.01	2.64
-0.01	-0.95	-9.80	-12.32	-0.02	2.86
0.17	-0.98	-9.88	-12.34	-0.02	3.16
0.22	-0.99	-9.91	-12.44	-0.03	3.06
				Average of the 6 values:	2.77
				2SD of the 6 values:	0.62

Negative saturation indexes (SIs) of $PbCO_3$(s) (cerussite) (Figure VIII-1A) means that the cerussite loaded to initiate the dissolution reaction cannot exist or became unstable under the posed experimental conditions, and has transformed to $NaPb_2(CO_3)_2(OH)$(s) (abellaite) through Reaction (1), which corroborates with the XRD scans (Figure VI-1). It is unclear whether Reaction (1) has proceeded via dissolution-precipitation or solid-state transformation because the measurements were not performed at the very beginning of the experiments, which was not the design scope of this solubility experiments to obtain thermodynamic model parameters at equilibrium. The observations, i.e., negative SIs of cerussite and the formation of abellaite on XRD (Excerpt VI-1, Excerpt VI-2, Figure VI-1), indicate the the SIT-log K of $PbCO_3$(s) = -2.85 (Table VIII-2) is accurate or, at least, useful in interpreting the experimental observations.

Information Only

The log Q calculated for abellaite, 2.77 ± 0.62 (Table VIII-3), can be assumed to be close to the log K of Reaction (8) for the following reason: Once Reaction (8) is included in Table VIII-2 with its log K ≡ log Q, the calculated SIs for abellaite would be aligned along zero with the same 2SD, indicating that the solution is in equilibrium with abellaite;

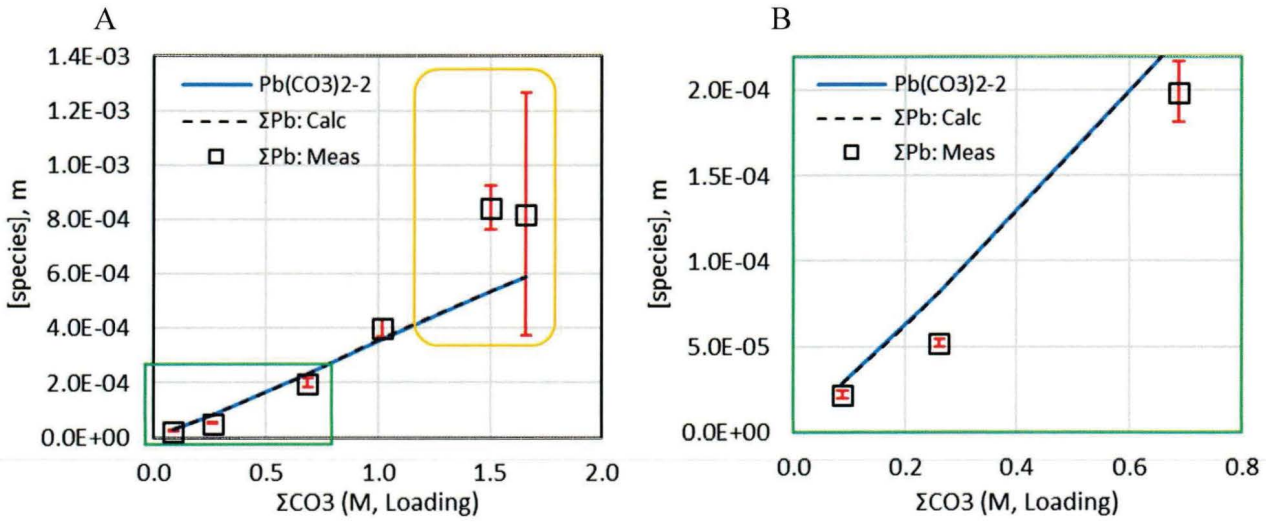
$$SI = \text{Log } Q - \text{Log } K, \text{ thus} \quad (10)$$

$$\text{If Log } Q \approx \text{Log } K, \text{ then } SI \approx 0, \text{ i.e., solubility equilibrium} \quad (11)$$

The calculation results are presented in Figure VIII-2. The residual, defined by Equation (12) below, is 0.119. Detailed speciation in log scale is illustrated in Figure VIII-3.

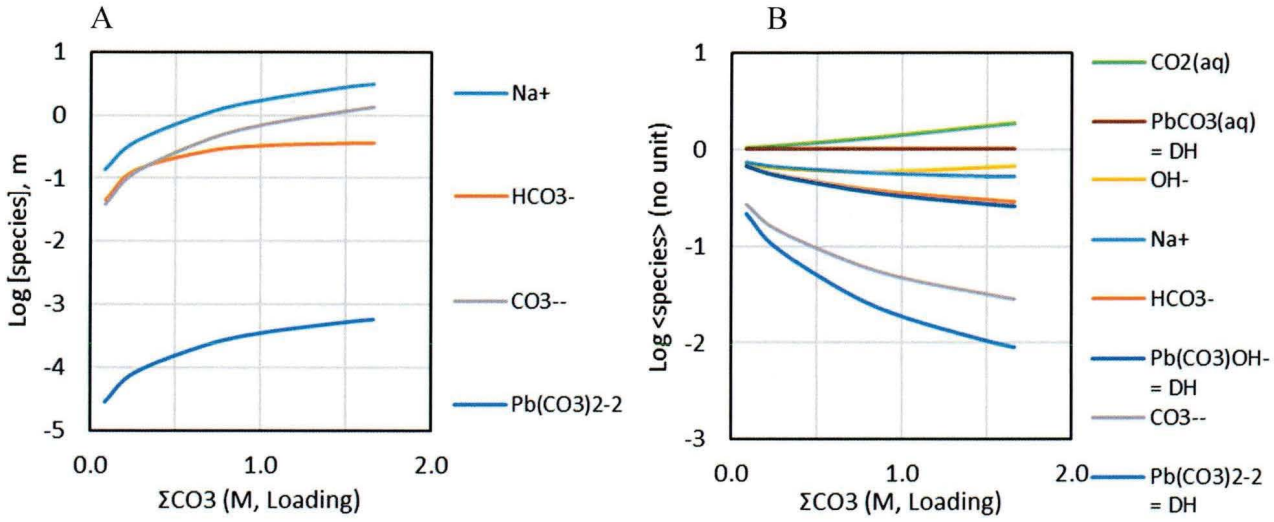
$$\text{Residual} = \Sigma(\text{Log } \Sigma\text{Pb:Calc} - \text{Log } \Sigma\text{Pb:Meas})^2 \quad (12)$$

Figure VIII-2. Measured ΣPb are compared with calculated ΣPb in equilibrium with $NaPb_2(CO_3)_2(OH)$(s) (abellaite). A. Whole range. B. Zoom-in view of the area marked with green rectangle. See text to find explanation for the area marked with orange rectangle.



Information Only

Figure VIII-3. A. Detailed speciation for Figure VIII-2. B. Plots of log <species> present in the experiments. Activity coefficients for additional species other than those in A are presented for comparison purpose. DH = Debye-Huckel values.



VIII.4. Fitting: Interaction vs. Cumulative Complexation

By assuming the accuracy of log K for $Pb(CO_3)_2^{-2}$ adopted from Powell et al. (2009), adjustment of the log K of Reaction (8), denoted log K(8) hereafter, seems warranted because the dashed line of the calculated ΣPb passes only one error bar (Figure VIII-2). Note that, however, the adjustment of log K(8) cannot make the slope of the dashed line change for better delineation in the area marked with orange rectangle. Adjustment of the log K(8) would shift the whole dashed line move up or down.

VIII.4.1. Interaction

One way to make the slope of the dashed line increase in the orange rectangle, i.e., at and above ΣCO3 loading of 1.0 M, is to assign PIPs to the major Pb(II) species, i.e., $Pb(CO_3)_2^{-2}$ (dark blue line in Figure VIII-2A and Figure VIII-3A), by pairing it with one of the ions of the background solutions, i.e., Na^+, HCO_3^-, CO_3^{-2} (Jang, 2019, AP-182). The PIPs need to be adjusted to decrease the activity coefficient of $Pb(CO_3)_2^{-2}$, so that the concentration of $Pb(CO_3)_2^{-2}$ increases at a given activity of $Pb(CO_3)_2^{-2}$.

The relationship of activity, concentration, and activity coefficient is defined in Equations (13) and (14). Without PIPs assigned to $Pb(CO_3)_2^{-2}$, the activity coefficients of $Pb(CO_3)_2^{-2}$, denoted

Information Only

<$Pb(CO_3)_2^{-2}$> hereafter, follow the Debye-Huckel values calculated by the Debye-Huckel term in PACE[13] (lower dark blue line in Figure VIII-3B);

$$\{species\} = <species> \cdot [species], \text{ by taking log on both sides,} \quad (13)$$

$$Log\ \{species\} = Log\ <species> + Log\ [species] \quad (14)$$

where {species}, <species>, and [species] mean, hereafter, the activity, activity coefficient, and concentration of the given species, respectively.

Candidate species pairs for such ionic interaction are $Na^+/Pb(CO_3)_2^{-2}$, $CO_3^{-2}/Pb(CO_3)_2^{-2}$, and $HCO_3^-/Pb(CO_3)_2^{-2}$. At ΣCO3 loadings above 1.0 M, $[Na^+]$ ranges from 1.76 to 2.98 M (Table IV-1), and the calculated $[HCO_3^-]$ and $[CO_3^{-2}]$ range from 0.32 to 0.36 and from 0.71 to 1.3 M.

The pair $Na^+/Pb(CO_3)_2^{-2}$ is selected for the fitting, because (i) $[Na^+]$ is higher than $[HCO_3^-]$ and $[CO_3^{-2}]$, and (ii) cation-anion interactions are assumed stronger than the same charge, i.e., anion-anion, interactions. The set of PIPs for $Na^+/Pb(CO_3)_2^{-2}$ consists of six values; $PIP(Na^+/Pb(CO_3)_2^{-2}) = (\alpha_1, \alpha_2; \beta^{(0)}, \beta^{(1)}, \beta^{(2)}, C^\phi)$. Among the six values, $\alpha_1 = 2.0$ and $\alpha_2 = 12.0$ for species pairs containing univalent ion(s) (Pitzer, 1991). α_2 does not materialize when $\beta^{(2)} = 0$ due to the construct of PACE (Harvie et al., 1984; Pitzer, 1991). This selection renders the PIPs for the remaining possible interaction pairs, $CO_3^{-2}/Pb(CO_3)_2^{-2}$ and $HCO_3^-/Pb(CO_3)_2^{-2}$, to be zeros, and their interactions would be collectively explained by the PIPs of $Na^+/Pb(CO_3)_2^{-2}$.

The ionic strength within the orange rectangle (Figure VIII-2A) ranges 2.6 to 4.6 m, thus, $\beta^{(0)}$, which effectively adjust the activity coefficient at such range of the ionic strengths, is selected to be fitted. To lower the prediction in Figure VIII-2B (i.e., in the area marked with the green rectangle in Figure VIII-2A), the log K of $NaPb_2(CO_3)_2(OH)$(s) (abellaite) (log K(8) in page 25) should be fitted simultaneously. The $\beta^{(0)}$ of $PIP(Na^+/Pb(CO_3)_2^{-2})$ would have little to no influence at the lower ionic strength. The results are presented in Figure VIII-4, and detailed speciation of the calculation is illustrated in Figure VIII-5. The residual reduced from 0.119 (Figure VIII-2) to 0.011.

[13] PACE: Pitzer Activity Coefficient Equation

Information Only

Figure VIII-4. Results of fitting (i) log K(abellaite) from 2.77 to 2.40, and (ii) $\beta^{(0)}$ of $Na^+/Pb(CO_3)_2^{-2}$ from 0.0 to -0.137. The residual reduced from 0.119 (Figure VIII-2) to 0.011.

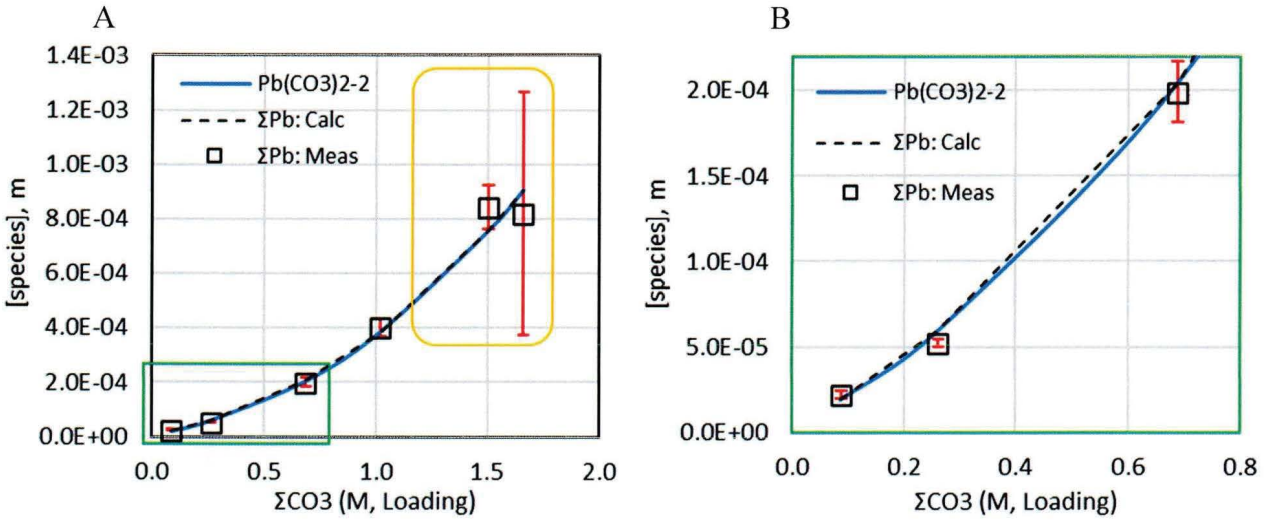
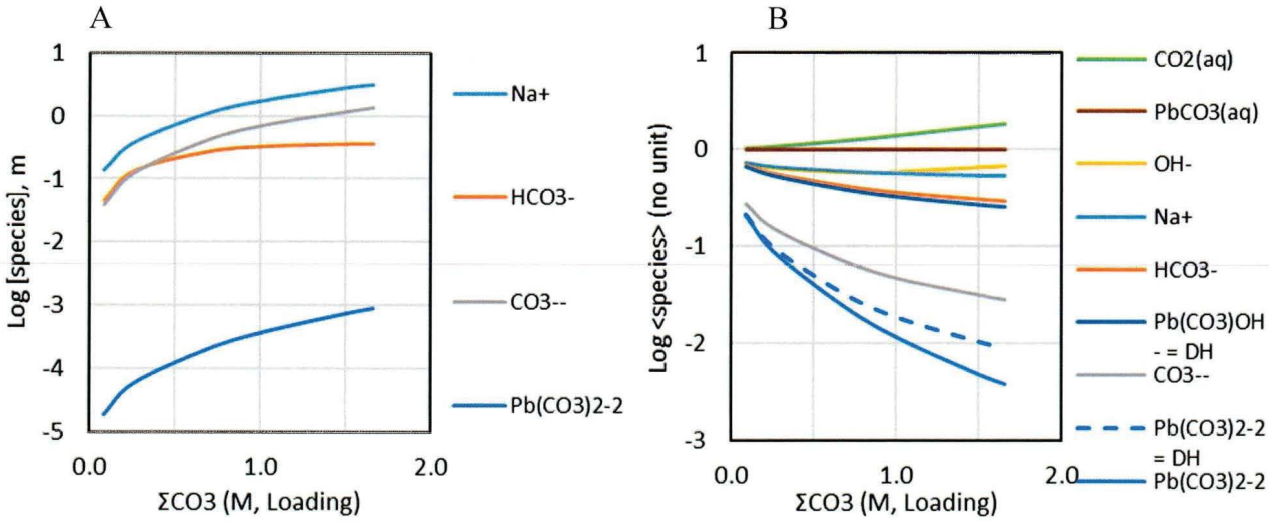


Figure VIII-5. A. Detailed speciation for Figure VIII-4. B. Plots of log <species> present in the experiments. Activity coefficients for additional species other than those in A are presented for comparison purpose. DH = Debye-Huckel values. Dashed blue line in B is the lower blue line in Figure VIII-3B. It is placed in B to compare $<Pb(CO_3)_2^{-2}>$ calculated by the DH term in PACE with $<Pb(CO_3)_2^{-2}>$ corrected by use of PIPs of $Na^+/Pb(CO_3)_2^{-2}$.



The new PIP($Na^+/Pb(CO_3)_2^{-2}$) = (2.0, 12.0; -0.137, 0, 0, 0) make the $<Pb(CO_3)_2^{-2}>$ smaller than the Debye-Huckel (DH) values, i.e., negative deviation of the $<Pb(CO_3)_2^{-2}>$ from the DH values in the log scale as illustrated by the lower blue lines in Figure VIII-3B and Figure VIII-5B. As a result, the

Information Only

concentration of $Pb(CO_3)_2^{-2}$, denoted $[Pb(CO_3)_2^{-2}]$ hereafter, increases by Equations (13) and (14) at the given activity of $Pb(CO_3)_2^{-2}$, denoted $\{Pb(CO_3)_2^{-2}\}$ hereafter. The $\{Pb(CO_3)_2^{-2}\}$ is defined by the log K (Table VIII-2).

The activity correction within the scheme of Harvie et al. (1984) makes the <species> increase from the DH values. This is illustrated in Figure VIII-3B. The activity coefficients for $CO_2(aq)$, OH^-, Na^+, HCO_3^-, and CO_3^{-2} are calculated by PACE using their respective PIPs in Harvie et al. (1984). The results of this calculation for their activity coefficients are consistent in that they are larger than the activity coefficients of the ions of the same |charge|[14] calculated without PIPs. That is, in Figure VIII-3B, the log $<CO_2(aq)>$ is more positive than the log $<PbCO_3(aq)>$ which follow the DH values. The logs of $<OH^->$, $<Na^+>$, and $<HCO_3^->$ are more positive than the log $<Pb(CO_3)OH^->$ which follows the DH values. The log $<CO_3^{-2}>$ is more positive than log $<Pb(CO_3)_2^{-2}>$ which follows the DH values prior to the fitting.

In Figure VIII-5B, the new PIP($Na^+/Pb(CO_3)_2^{-2}$) = (2.0, 12.0; -0.137, 0, 0, 0) makes the log $<Pb(CO_3)_2^{-2}>$ deviate negatively from the DH values. It is unclear to what properties of the species, $Pb(CO_3)_2^{-2}$, such an exceptional negative deviation can be attributed.

VIII.4.2. Cumulative Complexation

The common-ion effect on the solubility of $PbCl_2(s)$ in chloride solutions has been delineated by the cumulative complexation, the common-ion being Cl^- (Byrne and Miller, 1984; Millero and Byrne, 1984; Felmy et al., 2000; Jang, 2021c). A series of Pb^{+2} - Cl^- complexes, e.g., $PbCl^+$, $PbCl_2(aq)$, $PbCl_3^-$, were used to parameterize the solubility of $PbCl_2(s)$ in solutions of incremental ΣCl.

The experimental data being analyzed in this memo were generated in a chemical system where the common-ion is CO_3^{-2}. The positive deviation of ΣPb from the $[Pb(CO_3)_2^{-2}]$ in the orange rectangle of Figure VIII-2 can be explained by the cumulative complexation. Table VIII-2 lists the following Pb^{+2} - CO_3^{-2} complexes: $PbHCO_3^+$, $PbCO_3(aq)$, and $Pb(CO_3)_2^{-2}$. Their dominance changes as $[CO_3^{-2}]$ increases. If the three Pb^{+2} - CO_3^{-2} complexes cannot delineate the experimental observation, defining a higher order complex, such as Reaction (15), could be an option to better describe the observation, rather than defining PIP($Na^+/Pb(CO_3)_2^{-2}$) of limited physical meaning. This option would help avoid the need of explaining why the $<Pb(CO_3)_2^{-2}>$ become smaller than the DH values, unlike other ions.

[14] |charge|: absolute values of the charge

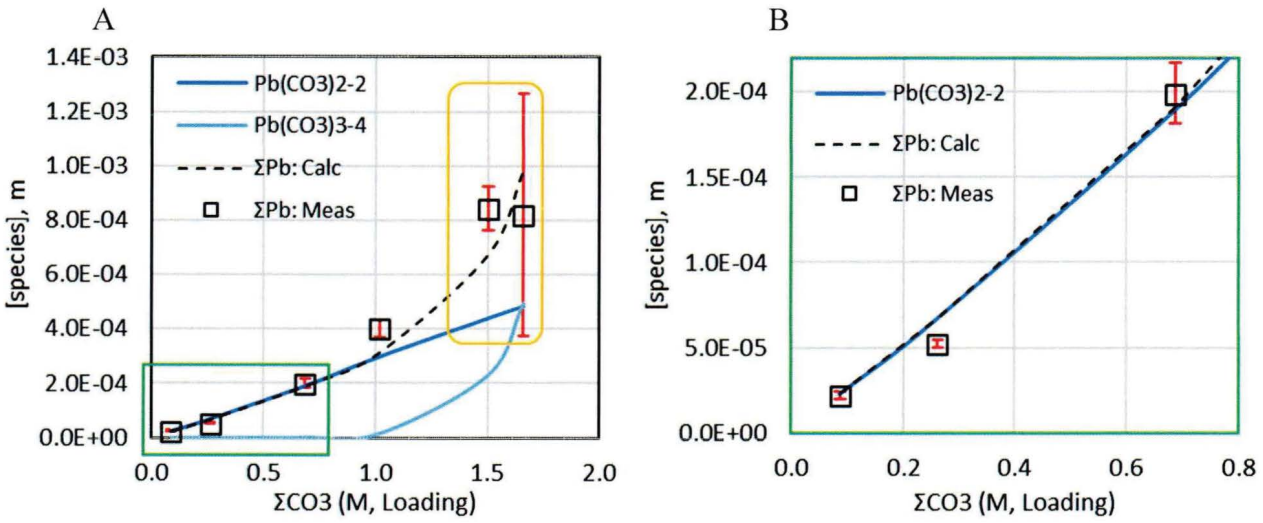
Information Only

557 $$Pb(CO_3)_3^{-4} + 3H^+ = Pb^{+2} + 3HCO_3^- \quad (15)$$[15]

558 Application of Reaction (15) in addition to the reactions in Table VIII-2 resulted in the prediction
559 presented in Figure VIII-6. The log K(15) and the log K(8) (abellaite) were fitted simultaneously as
560 was done in the simultaneous fitting of the PIP($Na^+/Pb(CO_3)_2^{-2}$) and log K(8) (abellaite).

561 Figure VIII-6. Results of fitting (i) log K(abellaite) from 2.77 to 2.59, and (ii) log K of
562 Reaction (15) to 27.19. The residual reduced from 0.119 (Figure VIII-2) to 0.041.

563



564

565 The interaction of $Na^+/Pb(CO_3)_2^{-2}$ could be considered purely hypothetical. Such interaction cannot
566 be isolated for measurements in a simple system using independent techniques, e.g., isopiestic, emf,
567 etc. Simply speaking, such salt, $Na_2Pb(CO_3)_2(s)$, is not available. Therefore, it is unclear if the fitted
568 PIP($Na^+/Pb(CO_3)_2^{-2}$) would have physical meaning. Same story is applicable for the remaining
569 species pairs, $CO_3^{-2}/Pb(CO_3)_2^{-2}$ and $HCO_3^-/Pb(CO_3)_2^{-2}$. The ionic interactions of species in the latter
570 two pairs would require tertiary systems to be measured.

571 In the meanwhile, the existence of the new species, i.e., Reaction (15), may have better chances to get
572 accepted or rejected. The higher order Pb^{+2} - Cl^- complexes were implemented by the spectroscopic
573 measurements of Byrne (1981) and Byrne and Miller (1984). It is highly recommended to perform
574 spectroscopic measurements on samples obtained from similar experiments in the future.

[15] Used the following reaction, $NaPb_2(CO_3)_2(OH)(s) + 4HCO_3^- = 2Pb(CO_3)_3^{-4} + Na^+ + 3H^+ + H_2O$, to read out an initial guess based on the concentrations at ΣCO3 = 1.69 m (Table VIII-1); Log $^cK(15)$ = 18.9 at pmH = 9.50, ΣPb = 8.18E-04, ΣCO3 = 1.69 m, ΣNa = 3.09 m, where $^cK(15)$ is a conditional equilibrium constant for Reaction (15) at the given concentrations of the components. Detailed calculation is based on mass action law, and not shown for brevity of this document.

Information Only

IX. Summary

IX.1. This Memo

The set of SIT-log Ks in Table VIII-2 (Powell et al., 2009) delineates the solubility of abellaite closely when the ionic strength is less than 2.5 m (i.e., ΣCO3 loading less than 1.1 M; Figure VIII-2), but the prediction stays outside the experimental uncertainty. The prediction was made without using the SIT-parameters, i.e., the ε's, for the species defined by the SIT-log Ks. The activity coefficients of the species were calculated by the Debye-Huckel term in the PACE implemented in EQ3NR (Wolery and Jarek, 2003). The activity coefficients of the ions in the background solutions were calculated in support of their respective PIPs (Harvie et al., 1984).

When an ionic interaction was assigned to the species pair of $Na^+/Pb(CO_3)_2^{-2}$, an improved fit resulted, but non-conventional behavior of $<Pb(CO_3)_2^{-2}>$ was observed (compare Figure VIII-3B and Figure VIII-5B). Difficulty in isolating and measuring such interaction in simple salt system, such as $Na_2Pb(CO_3)_2(s)$, was explained in the previous section, and an alternative was suggested, i.e., cumulative complexation.

To avoid the need to address the physical meaning of PIP($Na^+/Pb(CO_3)_2^{-2}$), a higher-order Pb^{+2} - CO_3^{-2} complex, i.e., $Pb(CO_3)_3^{-4}$ (Reaction (15)), was introduced under the concept of cumulative complexation. When its log K was fitted, an improved fit was obtained (Figure VIII-6). Spectroscopic identification of the new species is at least feasible, and could have better chance of success than isolating and quantifying the ionic interaction between Na^+ and $Pb(CO_3)_2^{-2}$ using the hypothetical salt.

SNL WIPP Geochemistry will investigate the SIT-log K(cerussite) = -2.85 using experimental designs where the formation of secondary lead carbonate solids, such as abellaite, can be effectively suppressed.

Likewise, the verification of log Ks for $PbHCO_3^+$, $PbCO_3(aq)$, $Pb(CO_3)_2^{-2}$ also require additional/new experiments specifically designed for such purpose. As such, for now, SNL WIPP Geochemistry does not have any evidence to exclude the log Ks of Powell et al. (2009) since they delineate the experimental observation within the uncertainty associated with the measurements in combination with the newly defined species, $Pb(CO_3)_3^{-4}$, without any new PIPs.

Table IX-1 lists the conclusion of this memo. No PIPs for Pb^{+2} - CO_3^{-2} complexes are included in the conclusion.

Information Only

Table IX-1. Reactions and the log Ks (25 °C, I = 0).

Reactions	Log K	Remarks
Aqueous Complexation		
$PbHCO_3^+ = Pb^{+2} + HCO_3^-$	-1.86 ± 0.1	Powell et al. (2009): Provisional (p.2429)
$PbCO_3(aq) + H^+ = Pb^{+2} + HCO_3^-$	3.88 ± 0.72	Powell et al. (2009): Indicative (p.2429)
$Pb(CO_3)_2^{-2} + 2H^+ = Pb^{+2} + 2HCO_3^-$	10.53 ± 0.24	Powell et al. (2009): Provisional (p.2429)
$Pb(CO_3)OH^- + 2H^+ = Pb^{+2} + HCO_3^- + H_2O$	13.42 ± 0.2	Powell et al. (2009): Statistically predicted (p.2441)
$Pb(CO_3)_3^{-4} + 3H^+ = Pb^{+2} + 3HCO_3^-$	27.19	This memo (Figure VIII-6)
Dissolution		
$PbCO_3(s)$ (Cerussite) $+ H^+ = Pb^{+2} + HCO_3^-$	-2.85 ± 0.07	Powell et al. (2009): Recommended (p.2429)
$NaPb_2(CO_3)_2(OH)(s)$ (Abellaite) $+ 3H^+ = Na^+ + 2Pb^{+2} + 2HCO_3^- + H_2O$	2.59	This memo (Figure VIII-6)

The log K(1) is now 2 × -2.85 + (-2.59) = -8.29. By the mass action law, the equation for the line dividing the stability fields of cerussite and abellaite is;

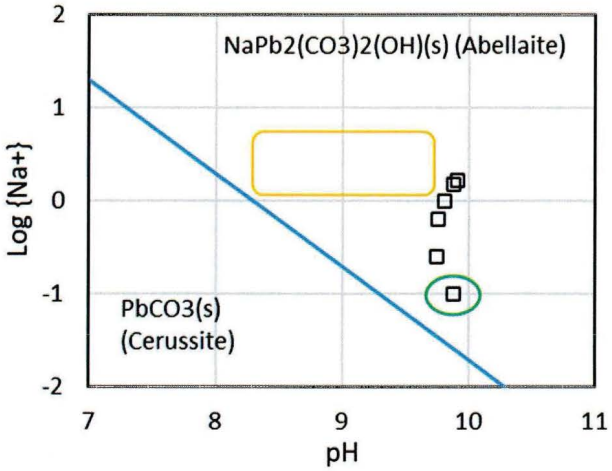
$$\text{Log } \{Na^+\} = -pH - \text{Log } K(1) - \log \{H_2O\} \quad (16)$$

where $\{Na^+\}$ and $\{H_2O\}$ are activity of Na^+ and water calculated for the six experimental conditions using the model in Harvie et al. (1984) and Table IX-1. The line of Equation (16) is presented as the blue one in Figure IX-1. With log $\{H_2O\}$ calculated ranging from 0.00 to -0.03, the thickness of the line is comparable to the uncertainty of the location of the line with respect to $\{H_2O\}$. The symbols in Figure IX-1 represent the six experimental conditions at equilibrium, and they indicate the stability of abellaite for all conditions. The data point marked with green oval represents the experimental condition at the lowest Na loading, where an overestimation of ΣNa possibly due to the low detection limit of the instrument was suggested to explain (i) the coexistence of cerussite and abellaite (Figure VI-1), and (ii) mass balance of ΣNa (Section VII) related to the large value of ΣNa recovery (Figure V-8B). If it truly represents an overestimation, the data point would approach closer to the blue line.

Because Reaction (1) is independent of the carbonate concentrations, the pH is the key player at a given $[Na^+]$ in determining the stability of cerussite vs. abellaite. Formation of abellaite from cerussite does not require elevated concentrations of carbonate based on the stoichiometry of Reaction (1). The orange rectangle in Figure IX-1 approximately locates the WIPP-relevant geochemical condition (pH ~9.0, 1 < $[Na^+]$ < 5 M), where the stability of abellaite is predicted over cerussite.

Information Only

Figure IX-1. Stability fields of cerussite and abellate in log {Na^+} vs. pH plane. The area marked with orange rectangle represents an approximate WIPP chemical conditions for {Na^+} and pH.



X. REFERENCES

X.1. A

Arnold, R., and J. Jang, 2022. Results of Temperature Monitoring in Three Gloveboxes in SNL WIPP NPHB. Memo to SNL WIPP Records Center, 1/6/2022. Sandia National Laboratories, Carlsbad, New Mexico, U.S.A. ERMS 576538.

X.2. B

Bilinski, H., and P. Schindler, 1982. Solubility and equilibrium constants of lead in carbonate solutions (25 °C, I = 0.3 mol dm^{-3}). Geochimica et Cosmochimica Acta, 46, 921-928.

Byrne, R. H., 1981. Inorganic lead complexation in natural seawater determined by UV spectroscopy. Nature, 09 April 1981, 290(5806), 487-489.

Byrne, R. H. and W. L. Miller, 1984. Medium composition dependence of lead(II) complexation by chloride ion. American Journal of Science, vol. 284, 79-94.

X.3. C

None

X.4. D

None

X.5. E

Edwards, R., R. D. Gillard, P. A. Williams, and A. M. Pollard, 1992. Studies of secondary minerals formation in the PbO - H_2O - HCl system. Mineralogical Magazine, 56, 53-65.

Information Only

X.6. F

Felmy, A.R., L.M. Onishi, N.S. Foster, J.R. Rustad, D. Rai, and M.J. Mason. 2000. An aqueous thermodynamic model for the Pb^{2+} - Na^{+} - K^{+} - Ca^{2+} - Mg^{2+} - H^{+} - Cl^{-} -SO_4^{2-} - H_2O system to high concentration: application to WIPP brines. *Geochimica et Cosmochimica Acta* 64(21):3615-3628.

X.7. G

None

X.8. H

Harvie, C. E., N. Møller, and J. H. Weare, 1984. The prediction of mineral solubilities in natural waters: The Na-K-Mg-Ca-H-Cl-SO_4-OH-HCO_3-CO_3-CO_2-H_2O system to high ionic strengths at 25°C. Geochimica et Cosmochimica Acta, 48, 723-751.

X.9. I

None

X.10. J

Jang, J., 2019. Analysis Plan for Derivation and Addition of Equilibrium Constants and Pitzer Interaction Parameters to the WIPP Geochemical Thermodynamic Database. Analysis Plan AP-182, Revision 0. Sandia National Laboratories, Carlsbad, New Mexico, U.S.A. ERMS 571074.

Jang, J., 2021c. Revisit to the Pitzer Geochemical Thermodynamic Model for the $PbCl_2$(s) - HCl - H_2O System. Memo to SNL WIPP Records Center and SNL WIPP Geochemistry, May 25, 2021. Sandia National Laboratories, Carlsbad, New Mexico, U.S.A. ERMS 575309.

Jang, J., 2022. Email to C. Miller on 3/15/2022 at 1422. Courtesy review of a Book Chapter on Engineered Barriers by Yongliang Xiong. ERMS 577780.

X.11. K

Kirkes, L., T. Olivas, J. Jang, S. Kim, and Y. Xiong, 2014a. Third Milestone Reports on Test Plan TP 08-02, “Iron, Lead, Sulfide, and EDTA Solubilities”, Sandia National Laboratories, Carlsbad, New Mexico, U.S.A., ERMS 561911.

Kirkes, L., T. Olivas, J. Jang, S. Kim, and Y. Xiong, 2014b. Third Milestone Reports on Test Plan TP 08-02, “Iron, Lead, Sulfide, and EDTA Solubilities”, Revision 1, Sandia National Laboratories, Carlsbad, New Mexico, U.S.A., ERMS 562645.

Kirkes, L., T. Olivas, J. Jang, S. Kim, and Y. Xiong, 2014c. Third Milestone Reports on Test Plan TP 08-02, “Iron, Lead, Sulfide, and EDTA Solubilities”, Revision 2, Sandia National Laboratories, Carlsbad, New Mexico, U.S.A., ERMS 562947.

Kirkes, L., and Y. Xiong, 2019. Solid Characterization Milestone Report on Test Plan TP 08-02, “Iron, Lead, Sulfide, and EDTA Solubilities”, Revision 1. Sandia National Laboratories, Carlsbad, New Mexico, U.S.A., ERMS 572290.

Information Only

Kirkes, L., and P. Hora, 2020. Third Milestone Report on Test Plan TP 12-02, "Experimental Investigation of Borate Interactions with Rare Earth Elements Under the WIPP Relevant Conditions at Sandia National Laboratories Carlsbad Facility". GEOC-20-04. Sandia National Laboratories, Carlsbad, New Mexico, U.S.A. ERMS 574511.

X.12. L

None

X.13. M

Miller, C., 2022. Request of Courtesy Review of a Book Chapter on Engineered Barriers by Yongliang Xiong. Email chain originating from R. C. Camphouse through P. E. Shoemaker, C. Miller to P. Domski, J. Jang on 2/24/2022 at 1316. ERMS 577779.

Millero, F. J. and Byrne, R. H., 1984. Use of Pitzer's equations to determine the media effect on the formation of lead chloro complexes. *Geochimica et Cosmochimica Acta* 48, 1145-1150.

X.14. N

None

X.15. O

None

X.16. P

Pitzer, K. S., 1991. Ion interaction approach: Theory and data correlation. In: Pitzer, K. S. (Ed.), *Activity Coefficients in Electrolyte Solutions, 2nd Edition*. CRC Press, Boca Raton, Florida.

Powell, K. J., P. L. Brown, R. H. Byrne, T. Gajda, G. Hefter, A.-K. Leuz, S. Sjoberg, and H. Wanner. 2009. Chemical speciation of environmentally significant metals with inorganic ligands. Part 3: The Pb^{2+} + OH^-, Cl^-, CO_3^{2-}, SO_4^{2-}, and PO_4^{3-} systems (IUPAC Technical Report), Pure Appl. Chem., Vol. 81, No. 12, 2425-2476.

X.17. Q

None

X.18. R

None

X.19. S

Shoemaker, P. E., 2022. Email chain on the courtesy review of a book chapter by Y. Xiong on Engineered Barrier where Y. Xiong and R. C. Camphouse claiming no tie to SNL WIPP Geochemistry in the book chapter. ERMS 577781.

Stumm, W., and J. J. Morgan, 1996. *Aquatic Chemistry*. John Wiley & Sons, New York.

Information Only

X.20. T

None

X.21. U

None

X.22. V

None

X.23. W

Wolery, T., and R. L. Jarek, 2003. Software User's Manual, EQ3/6, Version 8.0, 01/01/2003. ERMS 548926.

X.24. X

Xiong, Y., 2014. Experimental and Thermodynamic Modeling of $PbEDTA^{2-}$ Interactions in NaCl and $MgCl_2$ Solutions. Sandia National Laboratories, Carlsbad, New Mexico, U.S.A. ERMS 562877.

Xiong, Y., 2015a. Experimental and Thermodynamic Modeling Solubility of Cerussite, $PbCO_3$(cr), in the Carbonate System to High Ionic Strengths, Revision 1, Supersedes ERMS 561917. ERMS 564929

Xiong, Y., 2015b. Experimental determination of lead carbonate solubility at high ionic strengths: a Pitzer model description. Monatshefte für Chemie, 146(9), 1433-1443.

Xiong, Y., 2015c. "Experimental determination of solubilities of lead oxalate (PbC2O4), di-calcium ethylenediaminetetraacetic acid (Ca2EDTA(s)) in MgCl2-H2O system, and earlandite (Ca3[C3H5O(COO)3]2•4H2O) in NaCl-H2O and MgCl2-H2O systems, and their respective Pitzer interaction parameters. Revision 1, Supercedes ERMS 564844". Work Carried Out under Tasks 23, 28, 29, 30, 31 and 35 of AP-154: Analysis Plan for Derivation of Thermodynamic Properties Including Pitzer Parameters for Solubility Studies of Iron, Lead and EDTA. To be included in the AP-154 records package AP-154, Revision 2. Carlsbad, NM: Sandia National Laboratories. ERMS: 564948.

Xiong, Y., L. Kirkes, and C. Marrs, 2016. A Pitzer Model for Am(III)/Nd(III) Hydroxide Solubility in NaCl-H_2O at 298.15 K to High Ionic Strengths: Experimental Validation and Model Applications. Analysis Report, Sandia National Laboratories, Carlsbad, New Mexico, U.S.A. ERMS 567002.

Xiong, Y., L. Kirkes, and C. Marrs, 2017a. Long-Term Experimental Determination of Solubilities of Micro-Crystalline Nd(III) Hydroxide in High Ionic Strength Solutions: Applications to Nuclear Waste Management. Aquatic Geochemistry, 23, 359-375.

Xiong, Y., L. Kirkes, and T. Westfall, 2017b. Experimental determination of solubilities of di-calcium ethylenediaminetetraacetic acid hydrate [$Ca_2C_{10}H_{12}N_2O_8.7H_2O$(s)] in NaCl and $MgCl_2$ solutions to high ionic strengths and its Pitzer model: Applications to geological disposal of nuclear waste and other low temperature environments. Chemical Geology, 454, 15-24.

Information Only

749 Xiong, Y., L. Kirkes, J. Knox, C. Marrs, and H. Burton, 2018a. Experimental determination of stability
750 constant of ferrous iron borate complex [$FeB(OH)_4^+$] at 25 °C from solubility measurements:
751 Implications for transport of iron in reducing environments, Chemical Geology, 493, 16-23.

752 Xiong, Y., 2018b. Experimental determination of solubilities of lead oxalate (PbC_2O_4), di-calcium
753 ethylenediaminetetraacetic acid hydrate ($Ca_2EDTA.7H_2O(s)$) in $MgCl_2$-H_2O system, and earlandite
754 ($Ca_3[C_3H_5O(COO)_3]_2 \cdot 4H_2O$) in NaCl-$H_2O$ and $MgCl_2$-H_2O systems, and their respective Pitzer
755 interaction parameters. Revision 3, Supersedes ERMS 567810. Work Carried Out under Tasks 23,
756 28, 29, 30, 31 and 35 of AP-154: Analysis Plan for Derivation of Thermodynamic Properties
757 Including Pitzer Parameters for Solubility Studies of Iron, Lead and EDTA. To be included in the
758 AP-154 records package. ERMS 570088.

759 Xiong, Y., Y. Wang, G. Roselle, and S. Kim, 2021a. Lead/lead-alloy as a corrosion-resistant outer layer
760 packaging material for high level nuclear waste disposal. Nuclear Engineering and Design, 380,
761 111294.

762 Xiong, Y., 2021b. Experimental determination of solubilities of tri-calcium di-citrate tetrahydrate
763 [$Ca_3[C_3H_5O(COO)_3]_2 \cdot 4H_2O$], earlandite, in NaCl and $MgCl_2$ solutions to high ionic strengths.
764 Applied Geochemistry, 125, 104856.

765 Xiong, Y., 2022. Chapter 3: Geochemical Functions of Engineered Barrier Systems. Sandia National
766 Laboratories, Albuquerque, New Mexico, U.S.A. SAND2022-2827B. A chapter in a book unknown
767 to SNL WIPP Geochemistry as of 9/27/2022.

768 X.25. Y

769 None

770 X.26. Z

771 None

772 (No broken link found by Jay Jang on 12/2/2022. Total line number = 772 including this line)[16]

[16] If you find the underlined number not match with the line number, please let J. Jang (jjang@sandia.gov) know to fix the format of this document.

WIPP:4.4.2.2.1:PA:QA-L:558083
Information Only